Send Orders for Reprints to reprints@benthamscience.net

International Journal of Sensors, Wireless Communications and Control, **2021**, *11,* **00-00**

RESEARCH ARTICLE

Flexible, Piezoelectric Aluminum-Doped Zinc Oxide Energy Harvesters with Printed Electrodes for Wearable Applications

Muhammad Irsyad Suhaimi[a,b], Anis Nurashikin Nordin[a,*], Aliza Aini Md Ralib[a], Lai Ming Lim[b] and Zambri Samsudin[b]

[a]*Department of Electrical and Computer Engineering, Kulliyyah of Engineering, International Islamic University, Malaysia, Kuala Lumpur, Malaysia;* [b]*Manufacturing Technology& Innovation (MTI), Jabil Circuit SdnBhd, Phase 4, 56, Hilir Sungai Kluang 1, Bayan Lepas Industrial Park, 11900 Bayan Lepas, Pulau Pinang*

Abstract: ***Aims*****:** Recent advancements in sensing technology and wireless communications have accelerated the development of the Internet of Things (IoT) which promotes the usage of wearable sensors. An emerging trend is to develop self-sustainable wearable devices, thus eliminating the necessity of the user to carry bulky batteries. In this work, the development of a flexible piezoelectric energy harvester that is capable of harvesting energy from low frequency vibrations is presented. The target application of this energy harvester is for usage in smart shoes.

Objectives**:** The objective of this research is to design, fabricate and test an energy harvester on PET substrate using Aluminum Zinc Oxide as its piezoelectric layer.

Methods**:** The energy harvester was designed as a cantilever structure using PET/AZO/Ag layers in d_{33} mode which can generate large output voltages with small displacements. The electrodes were designed as an interdigitated structure in which two significant design parameters were chosen, namely the effect of gap between electrodes, *g* and number of inter-digital electrodes (IDE) pairs, *N* to the output voltage and resonant frequency.

Results**:** The sputtered AZO on PET showed c-axis orientation at 002 peak with 2 values of 34.45° which indicates piezoelectric behavior. The silver IDE pairs were screen-printed on the AZO thin film. Functionality of the device as an energy harvester was demonstrated by testing it, using a shaker. The energy harvester was capable of generating 0.867 V_{rms} output voltage when actuated at 49.6 Hz vibrations.

Conclusion**:** This indicates that the AZO thin films with printed silver electrodes can be used as flexible, d_{33} energy harvesters.

ARTICLE HISTORY

Received: August 10, 2020
Revised: October 29, 2020
Accepted: November 02, 2020

DOI:
10.2174/2210327911666210126123257

Keywords: Flexible electronics, energy harvesting, ZnO, Aluminum doped ZnO, silver electrode, piezoelectric.

1. INTRODUCTION

Numerous technological advancements in terms of power reductions [1-3], size [4-6], and cost [7–9] in the field of integrated circuit technology have catalyzed the rapid evolution of wearable devices. Unfortunately, these new advancements are still constrained by the current battery technology, which creates expensive, bulky, and short lifespan devices [10-12]. A promising alternative is the energy harvesting, where its technologies have potential in finding applications for various critical areas ranging from health [13-20], structural health monitoring [21-23], agriculture [19, 20], to localization [26], logistics [22, 23], and security [24-30].

Research and development on technologies of renewable energy harvesting (EH) began during the early 21st century [31]. Since then, numerous EH technologies have progressed and even successfully turned into hardware prototypes to serve as a proof of concept [32]. Many researchers have spent a significant amount of time and efforts to find new and realistic ways of obtaining energy harvesting solutions, for example, solar [33-35], thermoelectric [36-38], vibration [39-41], and radio frequency (RF) [42-44] to extend the device lifetime in various applications [29]. Usage of EH improves the sustainability of low power electronic devices, such as smart wireless sensor networks [45], smart mobile

*Address correspondence to this author at the Department of Electrical and Computer Engineering, Kulliyyah of Engineering, International Islamic University, Malaysia, Kuala Lumpur, Malaysia;
E-mail: anisnn@iium.edu.my

2210-3279/21 $65.00+.00

gadgets [46], and yields better operational lifetimes [47]. Solar cell is difficult for portable applications due to its cost, limited efficiencies and large area requirements [43, 44]. Portable thermoelectric devices also have problems achieving the desired temperature gradient due to its small size [50-52]. As an alternative, vibration-based energy harvesters is an ideal candidate for wearable devices as it is not limited by the factors mentioned earlier.

The vibration-based energy harvesters derive their energy from ambient vibration sources such as from a car engine compartment, clothes dryer, blender casing, and even from walking or running activity [53-56].Mechanical excitation can usually be converted into energy using any of these three transduction mechanisms: electromagnetic [52, 53], electrostatic [54, 55], or piezoelectric [56, 57]. Electromagnetic energy harvesters are capable of generating high voltage by capturing energy from the magnetic field. When miniaturized however, harvesting energy from a magnetic field with MEMS device is not a direct process and requires external voltage sources and a high frequency [58, 59]. Electrostatic energy harvesters also can produce high energy density. However, it requires a polarizing charge or voltage for an initial excitation [60-65].

Out of the three transduction mechanisms, piezoelectric energy harvesting devices provide more promising solution for wearables. This is because piezoelectric energy harvesters are capable of directly converting vibration into usable energy in both macroscopic and micro-scale applications [61, 62]. It also has the highest energy densities [57, 64].

The aim of this work is to design, simulate and fabricate the wearable EH which consists of d_{33} mode piezoelectric structures and the Aluminum Doped Zinc Oxide (AZO) as piezoelectric material sputtered on flexible PET substrate. The performance of the proposed device is measured in terms of resonance frequency, displacement, and output voltage [66-68].

The target application for this energy harvester is as a smart shoe. The current trend of using wearables for monitoring the number of steps in order to maintain a healthy lifestyle makes this application very suitable [69-72]. In addition to the basic step counter, wearables can also be used to track other physical activities such as running, sprinting, in which data such as speed, acceleration, pressure will benefit advanced users such as athletes and the coaches [73-75]. Having a self-sustainable power source like an energy harvester will provide increased benefits for the user such as longer battery life and reduced necessity of charging. With this application in mind, this proposed design targets resonance frequencies lower than 100Hz to match ambient frequencies generated by the human body which are typically below 100Hz [76-78].

The rest of the paper is structured as follows. Section 2 explains the design concept and simulation of the piezoelectric energy harvester device. Meanwhile, Section 3 discusses the fabrication process, characterization of the device, electromechanical testing, and measurements. Finally, the conclusion of the study is given in section 4.

2. DESIGN CONCEPT AND FINITE ELEMENT SIMULATION

2.1. Selection of Piezoelectric Material

One of the most important aspects of EH design is the choice of piezoelectric material as it affects its energy conversion efficiency. Lead zirconate titanate (PZT) [68, 69], zinc oxide (ZnO) [70, 71] and aluminum nitride (AlN) [72, 73] are some of the piezoelectric thin films that are commonly used for EH application. The choice of piezoelectric material highly depends on its capability to generate high output power. Piezoelectric thin film with high ratios of k^2/ε or coupling factor, k^2 over dielectric constant, ε has been reported to generate high output power [79-85]. Table **1** shows the comparison of three possible piezoelectric materials used for the EH application.

As shown in Table **1**, high k^2/ε ratios can be achieved by zinc oxide thin films, making them ideal for energy harvesting applications. Most importantly, ZnO thin film can be sputtered on a flexible substrate using a standard sputter deposition technique at a low temperature without compromising its piezoelectric properties [86]. Poling and post-deposition annealing are not required [87], making this choice of material ideal for fabrication on flexible substrates such as polyethylene terephthalate (PET) which has a low melting point [77, 78]. For this work, aluminum-doped zinc oxide, AZO thin films were used as they have been reported to improve the material's electrical properties and thermal stability [88-90]. In the previous work, we have demonstrated AZO energy harvester demonstrated the capability of generating output voltage of up to 1.61V at 7.77MHz resonance frequency when fabricated on a silicon substrate [91]. This work intends to utilize the same piezoelectric material but on flexible substrates for wearable applications. The pro-

Table 1. Comparison of three Piezoelectric materials [62].

Material	Coupling Coefficient, k	Dielectric Constant, ε	Ratio, k^2/ε	Density, p(kg/m^3)
Lead Zirconate titanate (PZT)	0.35	1,700	7.21 x 10^{-5}	7,500
Zinc Oxide (ZnO)	0.33	10.9	9.99 x 10^{-3}	5,606
Aluminum Nitride (AlN)	0.24	10.5	5.49 x 10^{-3}	3,260

posed design targets resonance frequencies below 100Hz to suit ambient frequencies produced by the human body, that is usually below 100Hz [77].

Table **2** shows the comparison of eight different piezoelectric EH devices. Work 1 produces 2V when actuated using normal gait movements of 1 Hz. The piezoelectric layer, PZT can generate high voltages at the expense of being a hazardous material, which is harmful to the environment especially during fabrication process. Polyvinylidene fluoride (PVDF) used in work 3 and 4 also produces high output voltages of 3.6V and 9V respectively but has the drawback of requiring poling after fabrication to induce piezoelectricity. In terms of output voltages, work 6, 7, and 8 can successfully harvest output voltages of 0.3 to 1.61 Volts. However, the resonant frequencies used in these works are too high: 30 kHz, 7.77 MHz, and 220 Hz respectively, making it unsuitable for applications that harvest energy from the environment and human movements. The resonant frequencies for the energy harvesters used in work 2 and 5 (48 Hz and 20-30 Hz) are in the desired low range of resonant frequencies. Unfortunately, these works utilize rigid substrates such as $SiO_2$and stainless steel foil, which are not flexible and unsuitable for wearable devices. The choice of using AZO material for this work yields good results, where 0.87 V_{rms} can be generated when the devices are actuated at 49.6 Hz. The devices were fabricated on flexible PET substrates, making it ideal for integration in wearable devices [92-96]

2.2. Cantilever Design Considerations

A key design element is the energy harvester structure. There are three kinds of structures that are typically used for piezoelectric energy harvesting, namely the diaphragm [97], cantilever [98] and doubly supported beam structures[99]. The cantilever structure is the most preferred as it can create a greater stress in the piezoelectric material and hence larger output energy at the same vibration level [100]. Within the cantilever beam, two modes of excitation are possible, d_{33} (in the z-direction) and d_{31} (in the x-direction) as shown in Fig. (**1a**).

In the d_{31} mode, stress is applied in the axial direction while the voltage is generated in the z-direction perpendicular to the stress[101,103]. To harvest energy, d_{31} mode devices require separate top and bottom electrodes to induce polarization in the thickness direction of the piezoelectric device. For the d_{33}mode, the applied force is parallel to the direction of the obtained voltage[102]. Stress is applied using interdigitated electrodes to realize an in-plane poling scheme as shown in Fig. (**1b**).

For this work, d_{33} mode, three-layer devices were fabricated with screen-printed silver interdigitated electrodes on AZO thin films sputtered on flexible PET substrate. d_{33}mode devices were selected as it produces smaller capacitance at low-level vibrations and hence larger output voltage compared to d_{31}devices [87, 88, 104]. The d_{33} piezoelectric mode is more sensitive capable of generating larger voltages than the d_{31} mode with the same displacement of the cantilever [85]. During vibration, the cantilever bends and charges the piezoelectric capacitor where the open-circuit voltage is proportional to the stress, σ and the gap between electrodes, *g*. Meanwhile, in d_{31} mode, the open-circuit voltage is dependent on σ and the thickness of the piezoelectric layer. As the gap between electrodes is easier to control than the thicknesses, this makes d_{33}devices better designed for energy harvesting applications. Another added advantage is that compared to d_{31}, the d_{33}coefficient is also usually two times larger than the d_{31}coefficient [85].

The resonant frequency of the piezoelectric energy harvester is one of the most important factors influencing the conversion efficiency of a device from mechanical energy to electrical energy [105]. The natural resonance frequency of the device should be matched to the ambient vibration frequencies in targeted applications to maximize the output power. For d_{33} cantilever structures, the natural frequency of the micro-generator can be expressed as [100]:

Table 2. Comparison of piezoelectric energy harvester devices.

Work	Piezoelectric Material	Substrate	Resonant Frequency	Output
1 [80]	PZT	Fabrics	1 Hz	2V
2 [92]	PZT	SiO_2	48 Hz	42.5 mV
3 [93]	PVDF	Silicone rubber	1 Hz	3.6 V
4 [94]	PVDF	PI	1Hz	9 V
5 [95]	PZT	Stainless steel foil	20 Hz to 30 Hz	300mV
6 [62]	AZO	Stainless steel	30 kHz	345.4 mV AC
7 [91]	AZO	Silicone	7.77 MHz	1.61V
8 [96]	AZO	PET	220-1025 Hz	1.55V
9 This work	AZO	PET	49.6 Hz	0.87 V_{rms} 1.22 V_{pk}

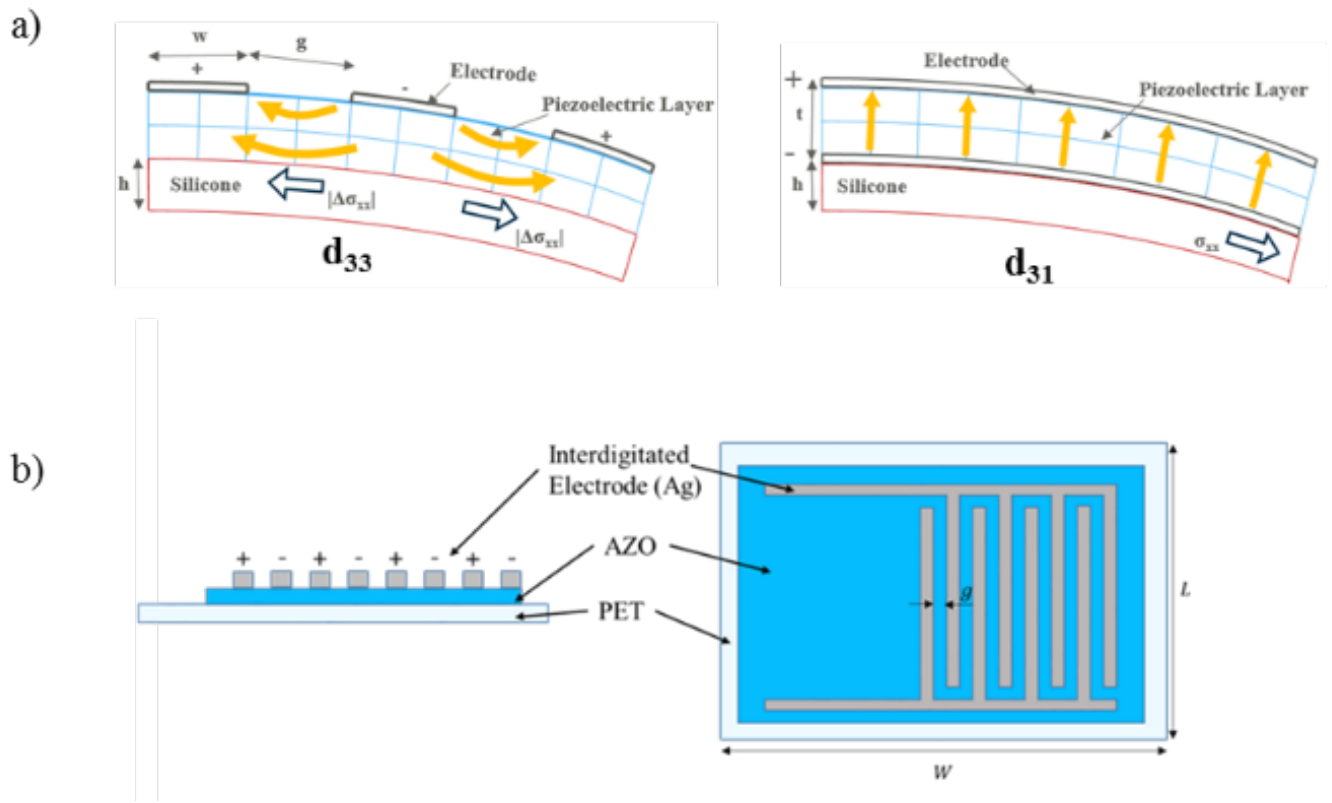

Fig. (1). (**a**) Concept of d_{33} and d_{31} mode of piezoelectric energy harvester. (**b**) The cross-section of the d_{33} piezoelectric device. (*A higher resolution / colour version of this figure is available in the electronic copy of the article*).

$$f_n = \frac{{V_n}^2}{2\pi}\sqrt{\frac{0.2636EI}{(L-l_m/2)^3(0.236mWL)}} \quad (1)$$

$$EI = \sum(Y_i I_i) = Y_s I_s + Y_p I_p \quad (2)$$

$$m = \rho_s t_s + \rho_p t_p \quad (3)$$

Where f_n is the nth mode resonant frequency, V_n is the nth mode eigenvalue, n=1, L is the length of the cantilever, l_m is the length of the proof mass, W is the width of the cantilever beam, Y is the Young's modulus, I is the area moment of inertia about the neutral axis, ρ_s is the density of the substrate, ρ_p is the density of piezoelectric material, t_s is the thickness of the substrate, and t_p is the thickness of the piezoelectric material.

Several design iterations were performed to determine the optimum values for the piezoelectric energy harvester. The devices were designed as wearable energy harvesters that harvest energy during walking and running movements which have reported frequencies between 25Hz to 100Hz [105, 106]. To attain this, the lengths and widths of the cantilever beam as well as the gap between the interdigital electrodes and the number of IDE pairs were varied. The material properties and physical parameter used for the theoretical calculations are summarized in Table **3** and Table **4.**

Equation **1** indicates that the cantilever's length plays a major role in tuning to the optimal resonant frequency. An inversely proportional relationship was observed as longer cantilever beams produce lower resonant frequencies. Fig. **2** shows the calculated resonant frequencies based on different lengths of the cantilever beam. For this work, the lowest calculated resonant frequency is 55 Hz for cantilever length of 0.023 m. This cantilever length was chosen as it lies within the frequencies of the human movement during walking and running(25Hz to 100Hz) [106].

Another crucial design parameter is the output voltage generated by the energy harvester [107]. The voltage on the load resistor of the power generator can be evaluated by equation 4 [100]:

$$V = \frac{Nd_{33}C_2 g/\mathcal{E}_{33}}{\sqrt{\left(2\varsigma {f_n}^2\right)^2 + \left({f_n}^2({k_p}^2/N) + (2\varsigma f_n/RC_p)\right)^2}} \quad (4)$$

where N is the number of interdigital finger pairs, d_{33} the piezoelectric constant, $\mathcal{E}_{33}$ the dielectric constant, C_2 the ratio of the stress of the piezoelectric layer to the vertical displacement of the proof mass, g the gap between the interdigital electrodes, ς the damping ratio, f_n the resonant frequency, k_p the electromechanical coupling coefficient, R the load resistor, and C_p the total capacitance between the electrodes.

2.2.1. Effect of IDE Pairs to the Output Voltage

As shown in Equation **4**, the output voltage is proportional to the number of IDE pairs, N as well as the gap between the interdigital electrodes, g. For this theoretical

Table 3. Material properties used for the theoretical calculation.

Material Properties	Symbol	Value	Unit
Density of PET substrate	ρ_s	1400	kgm^{-3}
Density of AZO thin film	ρ_p	5680	kgm^{-3}
Young's modulus of the substrate	Y_s	2.00×10^9	Nm^{-2}
Young's modulus of piezoelectric	Y_p	6.83×10^9	Nm^{-2}
piezoelectric constant	d_{33}	44.33	pmV^{-1}
Ratio of stress of the piezoelectric layer	C_2	1	-
Dielectric constant	ε_{33}	10.2	Fm^{-1}
Damping ratio	ς	0.05	-
Electromechanical coupling coefficient	k_p	0.33	-
Load resistor	R	120	kΩ
Total capacitance between the electrode	C_p	9.9	mF

Table 4. Design parameters used for the theoretical calculation.

Design Parameters	Symbol	Value	Unit
Thickness of substrate	t_s	175	µm
Thickness of piezoelectric	t_p	3	µm
Width of cantilever	W	23	mm
Length of cantilever	L	11, 14, 17, 20, 23	mm
Length of the proof mass	l_m	0	mm
Number of IDE pairs	N	1, 2, 3, 4	pairs
IDE gaps	g	0.4, 0.6, 0.8, 1.0 , 1.2	mm

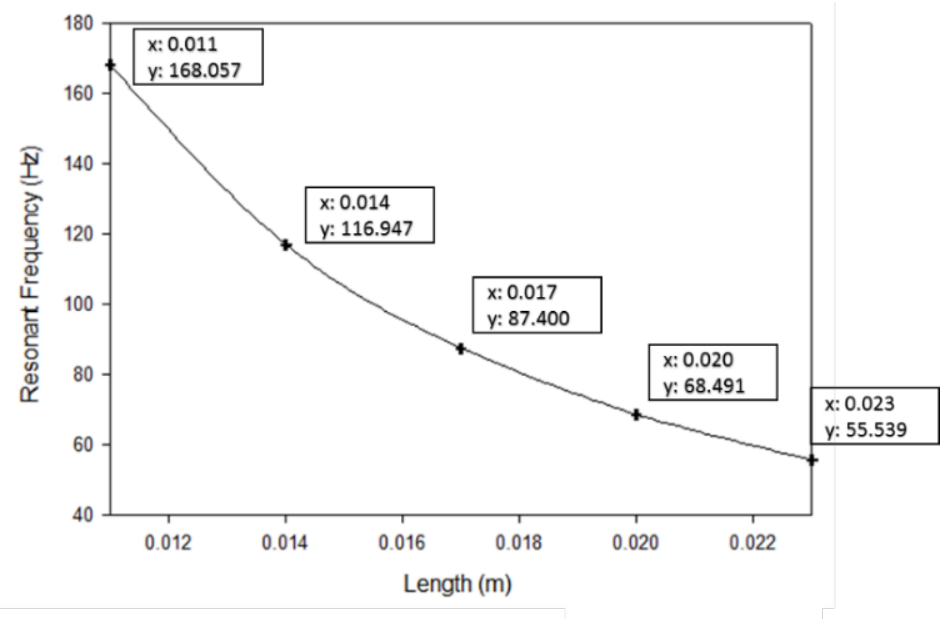

Fig. (2). Theoretical calculation of resonant frequency versus length of the cantilever beam.

calculation, the number of IDE pairs were varied from 1 to 4 with a fixed g = 0.4mm as shown in Fig. (**3**). The cantilever length also fixed to 0.023m as it will produce the lowest frequency as mentioned in the previous section. Other than that, the resonant frequency f_n is fixed to the calculated value at the previous section which is 55Hz. (Fig. **4**) shows that the highest number of IDE pairs which is 4 IDE pairs produces the highest output voltage.

2.2.2. Effect of the Gap Between Electrodes to the Output Voltage

Next, in order to identify the best gap between the electrodes, the number of IDE pair is fixed to 4 since it produces the highest output voltage of 21.743 mV_{rms}. The gap between the IDE pair varied from 0.4 mm to 1.2 mm as illustrated in Fig. (**5**) and the calculated output voltage is shown in Fig. (**6**). The resonant frequency also is fixed to the 55 Hz which is similar to the calculated value in the previous section. As predicted, larger gaps produce higher output voltages due to the lower capacitance values. Hence, based on the theoretical calculations, the optimum piezoelectric design is 0.023m in length, 4 pairs of IDE, and 1.2mm gap between electrodes. The number of IDE pairs is limited to 4 pairs and the gap is limited to 1.2mm in order to maintain the small size of the device which is 25mm by 25mm.

2.3. Finite Element Simulations

For more accurate design analysis, finite element simulation using COMSOL Multiphysics was performed to estimate the resonant frequency and the output voltage of the energy harvester [92 ,93]. COMSOL is a software framework, focused on methods of finite elements to model and simulate multiphysics applications using advanced numerical methods. COMSOL currently provides a major framework for electrical, mechanical, chemical, and fluid applications in physics and simulation.

Fig. (**7a-c**) illustrates the two-dimensional model of the energy harvester. The finite element model subdivides the device into smaller domains to ease the computation of governing equations of interest using a set of functions defined over each element. For this model, the mesh sequence type was set to 'Physics-controlled mesh' with 'Normal' element size. Using this method, the simulated result will be closer to the true solution.

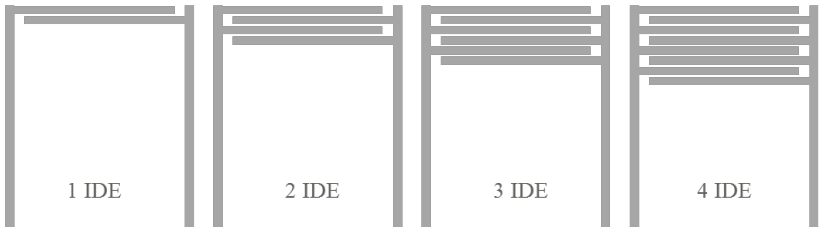

Fig. (3). Electrode design with different number of IDE pair for the theoretical calculation.

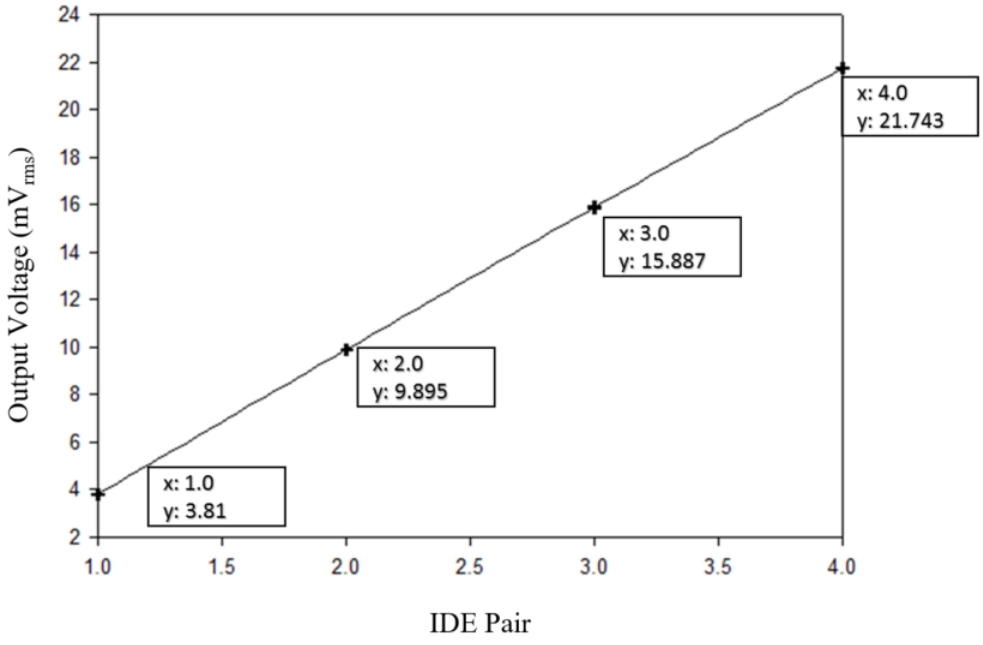

Fig. (4). Theoretical calculations of the output voltage versus the number of IDE pair.

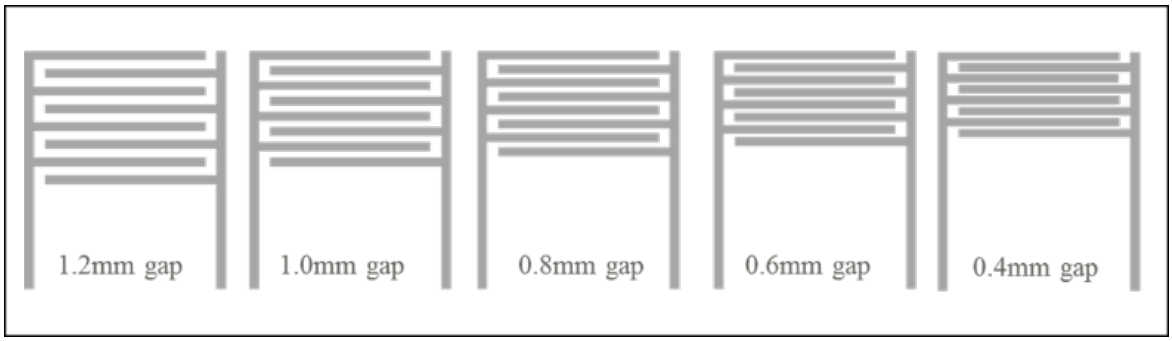

Fig. (5). Electrode design with the different gap between electrodes for the theoretical calculation.

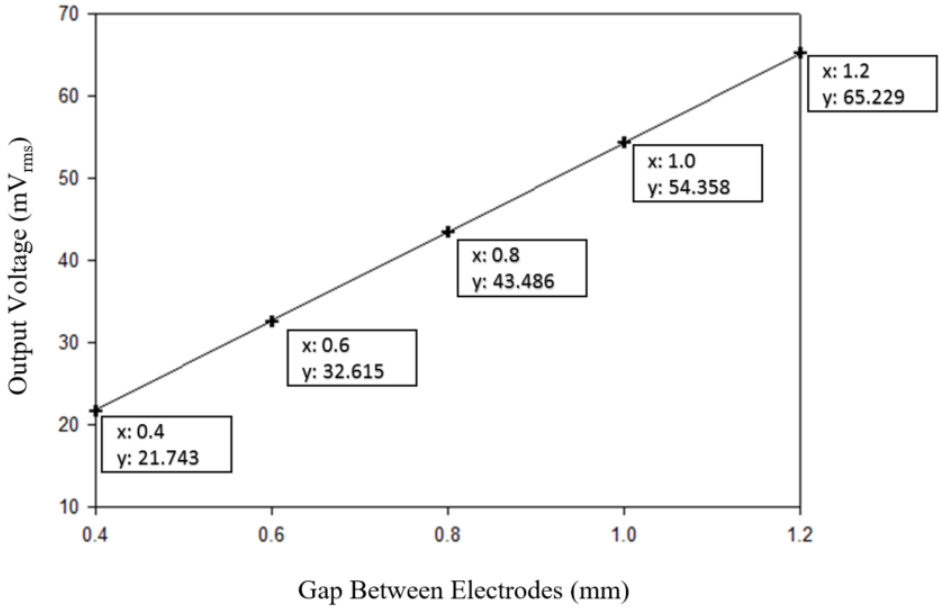

Fig. (6). Theoretical calculations of the output voltage versus the gap between electrodes.

Two types of analysis were performed namely Eigen frequency analysis to determine the device's resonance frequencies and electrostatic analysis to determine the output voltages and displacement. The resonance frequency lies at the highest vibration displacement and will thus provide the energy harvester with the maximum output power.

Table **5** shows the design parameter for the simulation work. The thickness of the electrode was set to 0.03 mm as a tradeoff between having high conductivities and the limitations of the printing process. The conductivity of the electrode will be increased if the thickness of the electrode is higher since the volume of the silver particle will also be increased. However, if the thickness is too high, it will lead to smearing of the Ag ink. After several runs of printing the electrodes, the thickness of 0.03 mm was found to be optimum as the thickness of the electrode is controlled at this value. The cross-sectional view of the model is shown in Fig. (**7a**).

Eigen frequency analysis was performed for the piezoelectric devices to analyze the structure's resonance modes. The dimensions for the PET and the dimension of AZO are both summarized in Table **5**. These dimensions are used by following the same dimension used in the theoretical measurement in order to get close and accurate desire result of output voltage and resonant frequency. The cantilever beam is fixed at one end side, while all the other regions have been set free to allow bending. Fig. (**7c**) presents the simulation results of the generated output voltage and the displacement at the resonant frequency. It shows that the highest displacement of 1.155mm with 0.065 V_{rms} output voltage occurs at 48.55Hz or the resonant frequency

To verify and refine the theoretical calculations, the next simulations are divided into two sections which are the 1) effect of the gap between electrodes to the output voltage and the resonant frequency and 2) the effect of IDE pairs to the output voltage and the resonant frequency. For this section, the resonant frequency will not be fixed to a certain value since the result will appear with the output voltage at the same time. It will totally depend on the design and properties that were inside the simulation.

2.3.1. Effect of Gap between Electrodes to the Generated Output Voltages and the Resonant Frequency

Similar to the theoretical analysis, the IDE gap was varied from 0.4mm to 1.2mm with the number of IDE pairs

Table 5. Simulation parameters and device dimensions.

Design Parameter	Value	Unit
PET Young's Modulus	3.6×10^9	N/m^2
AZO Young's Modulus	6.83×10^9	N/m^2
Ag Young's Modulus	22.1×10^9	N/m^2
PET density	1400	kg/m^3
AZO density	5680	kg/m^3
Ag density	8900	kg/m^3
PET Poisson ratio	0.3	Nil
AZO Poisson ratio	0.2	Nil
Ag Poisson ratio	0.33	Nil
PET dimension	23 x 23 x 0.175	mm
AZO dimension	18 x 18 x 0.003	mm
Ag dimension	14 x 14 x 0.030	mm

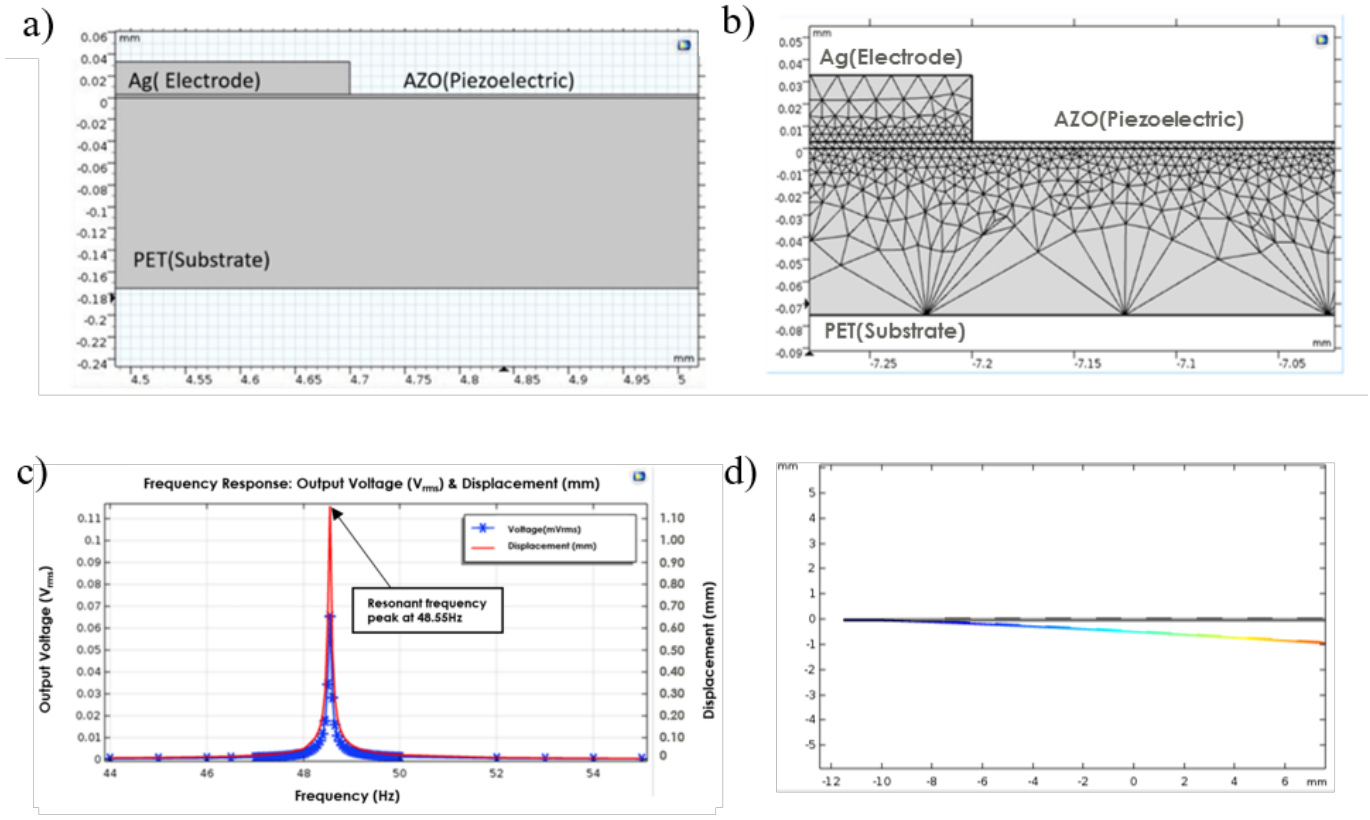

Fig. (7). (**a**) Cross-sectional view of piezoelectric cantilever design (**b**) Mesh of the device (**c**) Simulation results of output voltage and displacement of the energy harvester versus frequency (**d**) cantilever simulation results of displacement versus x at Mode 1 with resonant frequency of 48.55Hz.

fixed to 4 pairs. Fig. **8** shows the simulation results which indicate that the output voltage is higher when the gap is larger. Increasing the gap between the comb fingers is an effective method to increase output voltage for d_{33} piezoelectric mode [104]. Larger gaps or spacing between electrodes allow capturing higher output voltages *via* a larger effective

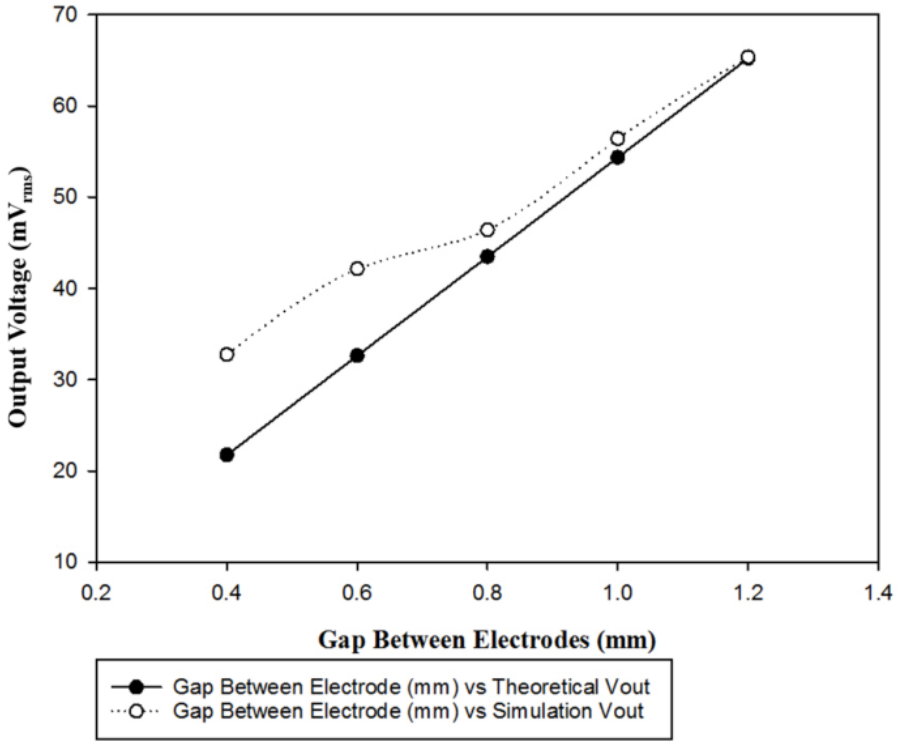

Fig. (8). The effect of the gap between electrodes to the output voltage.

area of the AZO layer. The highest output voltage of 65.34 mV_{rms} is attained when g = 1.2 mm. This is also in agreement with the theoretical value of the maximum output voltage of 65.229 mV_{rms}. The resonant frequency remains constant at 49Hz with different gaps, indicating that changing the gap between electrodes does not give a significant effect on the resonant frequency.

2.3.2. Effect of the Number of IDE Pairs to the Output Voltage and the Resonant Frequency

For this simulation, the gap between the electrodes will be the constant variable. It is fixed to 1.2 mm as it gives the highest output voltage in the previous simulation section. The variable value for the first category is the number of IDE pairs which is varied from two to four pairs as shown in Fig. (**3**). The simulation results are summarized in Fig. (**9**).

Based on the simulation results, it can be seen that the output voltage increases when the number of IDE pairs increases. This also agreed with the trend shown by the theoretical calculation. Fig. **10** shows the effect of IDE pairs on the resonant frequency. The resonant frequency of the device will be lower when the number of IDE pair increase. This might be due to the weight of the device increase when the number of IDE pairs increases since the mass of the device is indirectly proportional to the resonant frequency based on the formula in the theoretical calculation section. However, that formula in Equation **3** only considers the mass of the substrate and piezoelectric material which lead to the same value of resonant frequency when the number of IDE pairs increases.

2.4. Proposed Piezoelectric EH Design

The next step after simulation is the proposed piezoelectric EH design for fabrication. The electrode was designed based on the simulation geometry design since the simulation result agreed with the theoretical concept. The size of the electrode, the number of IDE pairs, and the gap between electrodes were fabricated according to the finalized design as shown in Table **6**. The electrode was designed using Solidworks software. The configuration of the electrodes was shown in Fig. (**3**) and Fig. (**5**).

3. EXPERIMENTAL WORK

3.1. Deposition of AZO Using RF Magnetron Sputtering

The technique of piezoelectric deposition comprises of various processes, such as sputtering techniques [108-110], chemical vapour deposition (CVD) methods [111] and spin on sol-gel deposition [112]. RF Magnetron sputtering process capable in preparing a highly aligned AZO on a substrate [62]. RF Magnetron sputtering is a powerful method as it permits low temperature deposition, enhances adhesion and exhibits uniform AZO at high deposition rates [113]. AZO can be prepared using a variety of methods, including CVD and sputtering process. The AZO deposition was done using ULVAC RF Magnetron sputtering machine at Kulliyyah of Engineering, IIUM.

A 3-inch diameter Aluminum doped Zinc Oxide target 2 wt% Al_2O_3 was used during the sputtering process. Polyethylene terephthalate (PET) with a thickness of 175 microns

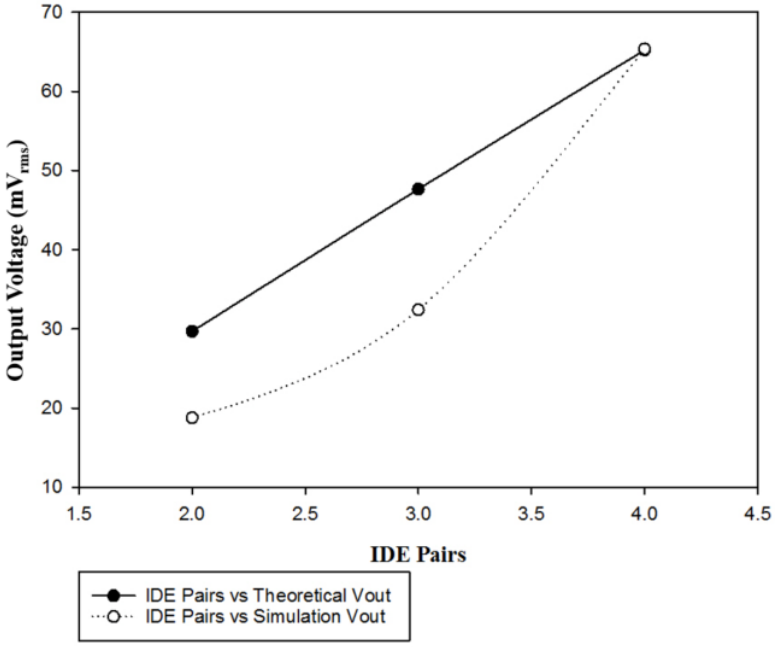

Fig. (9). The effect of IDE pairs to the output voltage.

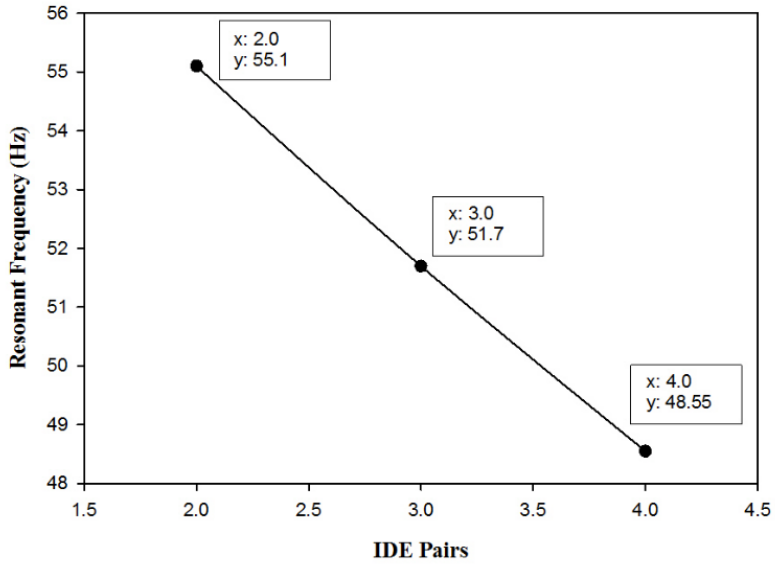

Fig. (10). The effect of IDE pairs to the resonant frequency.

was used as the substrate. The deposition chamber was initially vacuumed until the total base pressure of 3×10^{-4} Pa was attained. Sputtering was performed in pure argon by providing 250 WRF power at 13.56 MHz. As 20 sccm of Ar gas was incorporated, the working pressure was controlled at 0.667 Pa. The AZO thin film then was sputtered on Polyethylene terephthalate (PET) substrate for about 75 minutes at room temperature. The sputtering setups are summarized in Table **7** and the image of the sample after the sputtering process is shown in Fig. (**11b**).

3.2. Fabrication of Electrode Using Screen Printing Technique

Screen printing is widely used especially for electrode fabrication [114]. There are a few important things that need to be prepared for screen printing process include screen mesh design, types of ink and substrates, printing parameter, and curing to ensure the adhesion of ink to the substrate [115]. A 230 thread / inch polyester mesh with an emulsion thickness of 20 μm and a 25 N tension screen mesh has been used to screen-print the electrode using an automatic DEK

printer at MTI Lab, Jabil Circuit Sdn. Penang, Bhd. Prior to printing, silver ink with 70% metal loading (AST6400) from Gwent Group was mixed and defoamed at 600 rpm and 700 rpm respectively for 30 seconds using a centrifugal mixer (Thinky Mixer Model ARE-310). This is to ensure the ink is homogenous and to get rid of trapped air. Fig. (**11c**) shows the sample after printed with silver ink.

Table 6. Finalized design parameters.

Design Parameter	Value	Unit
Substrate (PET) thickness	175	µm
Substrate (PET) dimensions	23 x 23 x 0.175	mm
Piezoelectric (AZO) thickness	3	µm
Piezoelectric dimension	18 x 18 x 0.003	mm
Electrode material	Ag	Nil
Electrode thickness	30	µm
IDE gaps	1.0, 1.2	mm
IDE pairs	2, 3, 4	pairs

Table 7. Sputtering parameters.

Sputtering Parameter	Conditions
Target	AZO target 2 wt% Al_2O_3
Gas flow	20 sccm Ar gas
Substrate temperature	Room temperature
Base pressure	3×10^{-4} Pa
Substrate	PET
RF power	250W
Deposition time	75 min

The silver ink was cured in a conventional oven (ConthermThermotec 2000) at 120 °C for 45 minutes. Fig. (**11a**) describes the fabrication sequence of the piezoelectric device and Fig. (**11c**) indicates the image of the fabricated device.

3.3. Characterization of Materials

3.3.1. X-Ray Diffraction (XRD) Analysis

Usually, for obtaining high piezoelectric coefficients, ferroelectric materials need polarization [116]. Polarization can be obtained by implementing high electrical fields to produce electrical dipoles in the material [117]. AZO was selected as a piezoelectric material in this work, because it does not require poling [91]. AZO thin film produced with RF magnetron sputtering was reported to exert thin films with hexagonal wurtzite crystal structure with a well oriented c-axis in the 002 direction , making it piezoelectric [113]. The XRD measurements for this work were performed at Analytical Lab, MJIIT UTMKL using Panalytical X-ray Diffractometer. This machine examines the crystal's atomic and molecular structure. The incident X-rays beam that emits to the crystalline atoms will be diffracted into numerous specific directions and a 3D image of the electrons density can be obtained by calculating the angles and intensities of these diffracted beams. From this electron density, the crystal structure of the atom and its chemical bonds can be identified [118].

Fig. **12** depicts XRD experimental measurements of the RF Magnetron-sputtered AZO layer on the PET substrates where the ZnO (002) peak c-axis orientation can be clearly seen at 34.45 °. The ZnO peak full-wave half maximum (FWHM) was evaluated at 0.2558 which is very narrow. The lower the FWHM, the bigger the crystal size which makes the quality better [119]. This ensures that the sputtered AZO reveals the presence of ZnO(002) which is piezoelectric because the peak is close to ZnO orientation (34.4°) [91]. Al_2O_3 peak also is observed at 26.18° and its FWHM was measured to be 0.7675 [120].

3.3.2. Field-Emission Scanning Electron Microscopy (FESEM) and Energy Dispersive X-Ray (EDS) Analysis

The piezoelectricity of this device depends on the quality of the ZnO films [121]. FESEM was used to clarify the Ag and AZO layers cross-sections on PET substrate. The EDS was used to evaluate the ratio of atom composition of Ag/AZO/PET. The FESEM and EDS analysis for this work was performed at Usains Biomics Lab, USM Nibong Tebal, using Extreme High Resolution Field Emission Scanning Electron Microscope (XHR-FESEM) Model FEI Verios 460L.

Fig. (**13a**) shows the cross section of the Ag and AZO layer on PET. The columnar ZnO structures are perpendicular to the substrate and can be seen clearly in that figure. The presence of the columnar structures indicates a high probability of piezoelectricity in the AZO layer. The thickness of the piezoelectric film was also measured using FESEM. Fig. (**13b**) and Fig. (**13c**) below illustrate the cross-section of the piezoelectric films. The thickness of each layer is summarized in Table **8**.

The atom composition ratio of Ag/AZO/PET was displayed in Fig. (**14a**) and Table **9**. The EDS analysis proved the presence of Zinc, Oxygen, Silver, and Aluminum in the fabricated sample. The distribution area of the Zn and Ag elements were also depicted in Fig. (**14b**) below.

3.3.3. Piezoelectric Constant (d_{33}) and Sheet Resistivities

The d_{33} piezoelectric constant for each sputtered AZO layer was measured using a Model ZJ-6B quasi-static d_{33}/d_{31}meter. This measurement method is applicable for numerous kinds of piezoelectric material, including ceramics, crystals, and polymers [122]. The average measured d_{33} constant value was 1.8 pC/N and was found to be within the reported values of measured AZO piezoelectric constant of 0.02 pC/N to 5.27 pC/N [123].

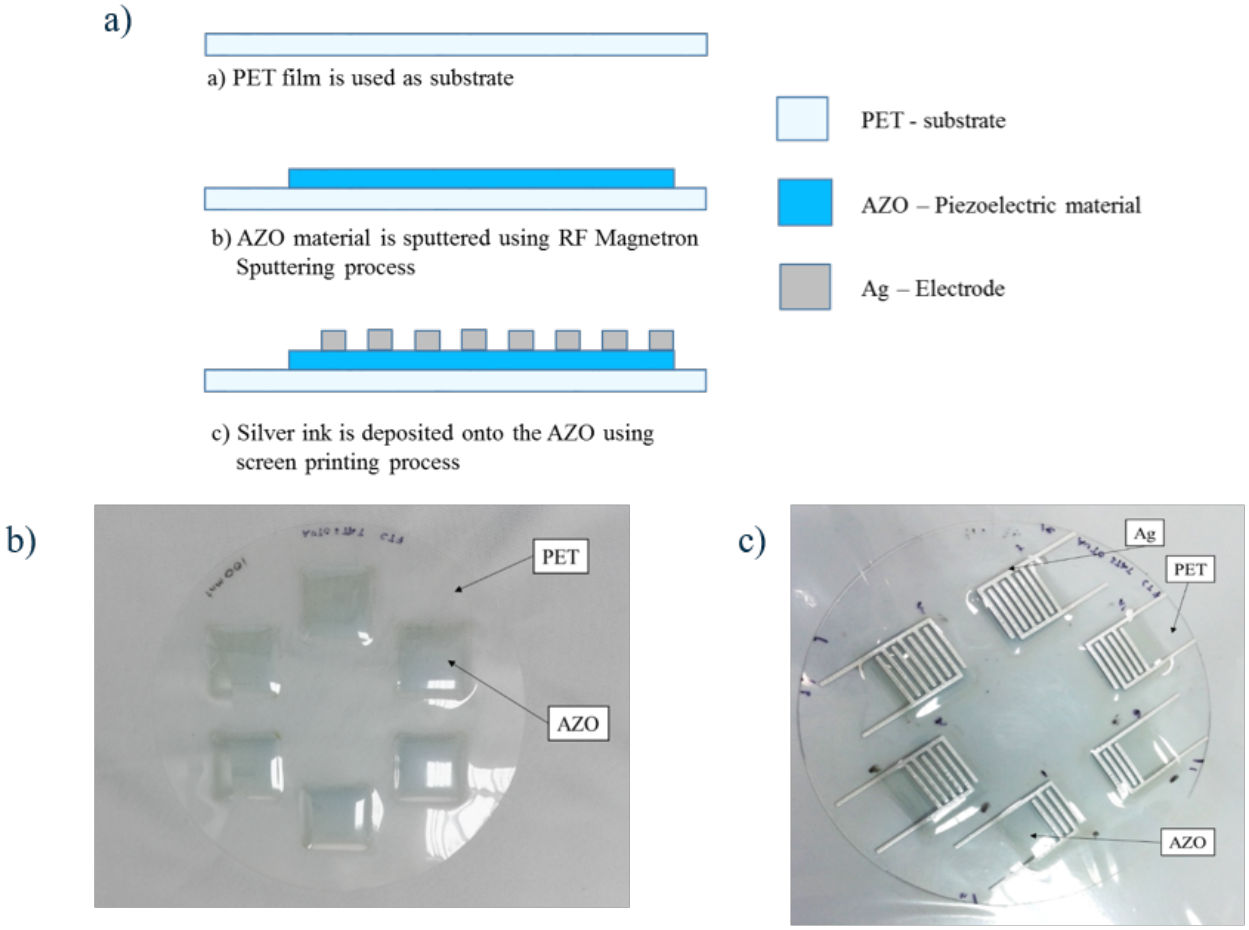

Fig. (11). (**a**)Fabrication sequence, (**b**) Sputtered AZO on PET substrate (**c**) Screen-printed electrode on top of AZOthin film. (*A higher resolution / colour version of this figure is available in the electronic copy of the article*).

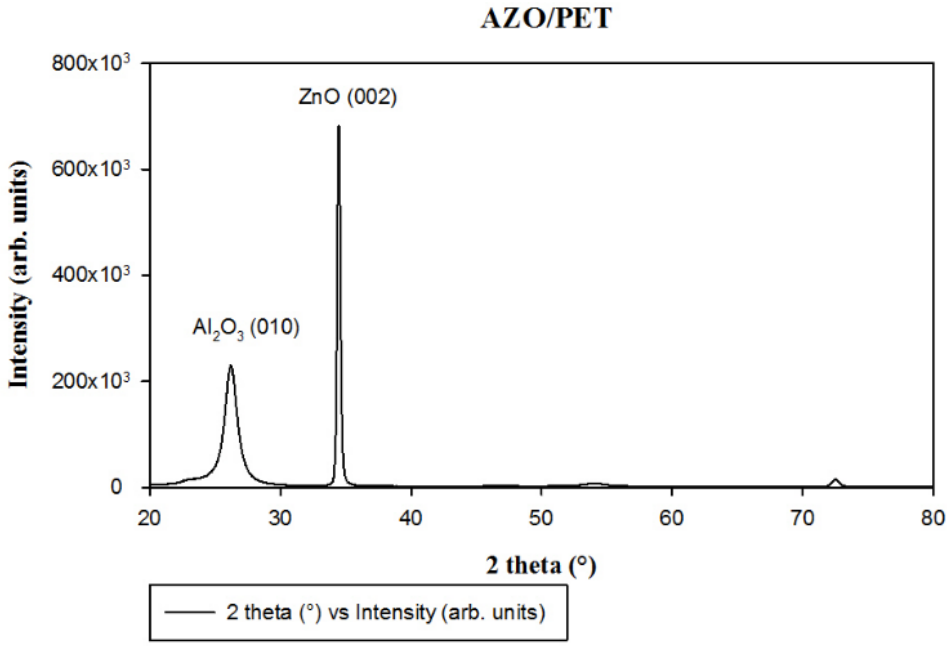

Fig. (12). XRD measurements performed on the AZO/PET layers.

Table 8. Energy harvester layer thicknesses.

Layer	Thickness (µm)
PET	175.5
Ag	24.9
AZO	1.86

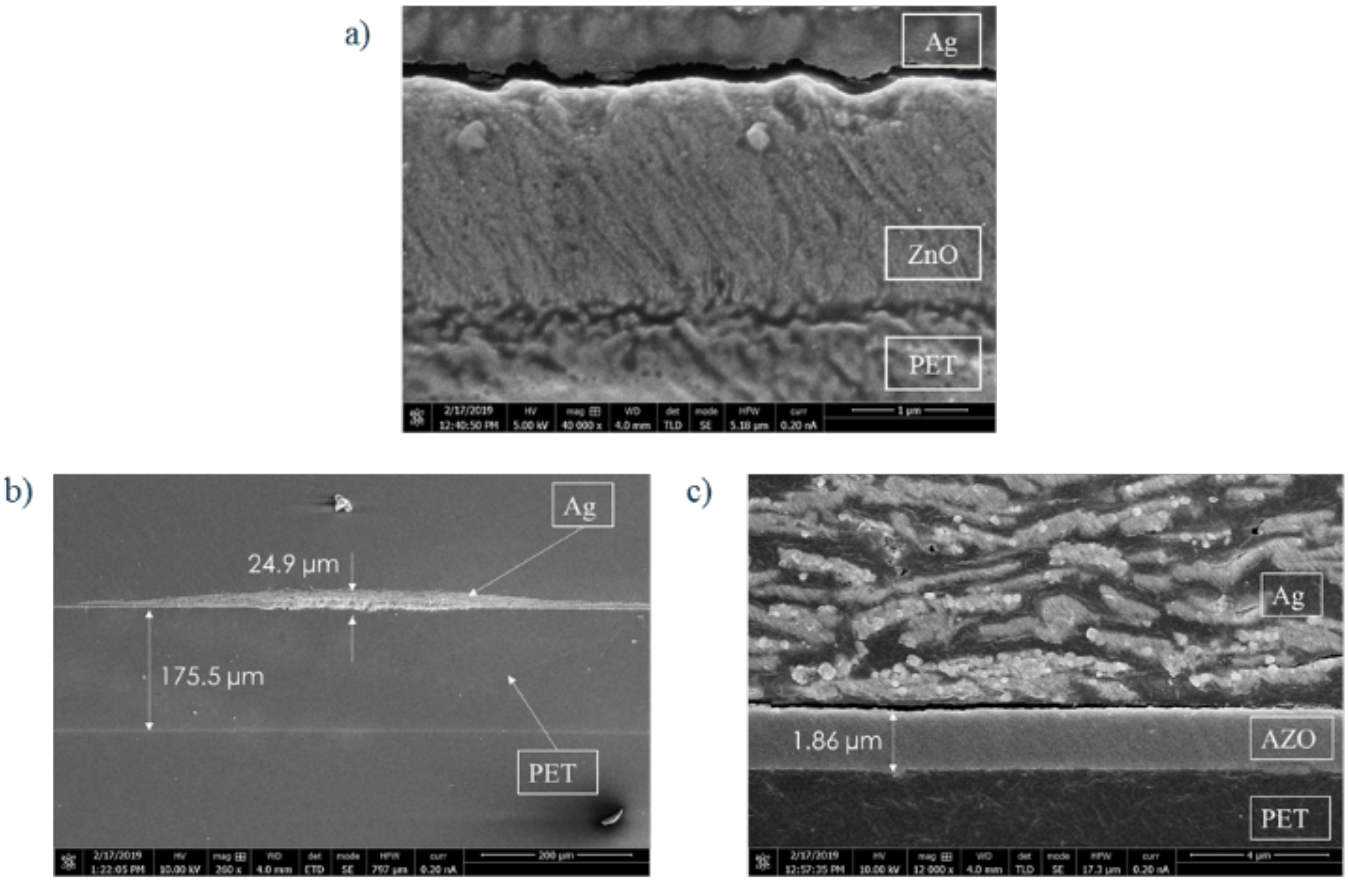

Fig. (13). (**a**) Columnar ZnO structures in the AZO layer (**b**), (**c**) Cross-section of the piezoelectric films.

Table 9. EDS analysis.

Element	Weight (%)	Atomic (%)
C	30.28 ± 0.36	59.86
O	18.45 ± 0.39	27.38
Al	0.04 ± 0.08	0.03
Zn	10.13 ± 0.31	3.68
Ag	41.11 ± 0.47	9.05
Totals	100.00	100.00

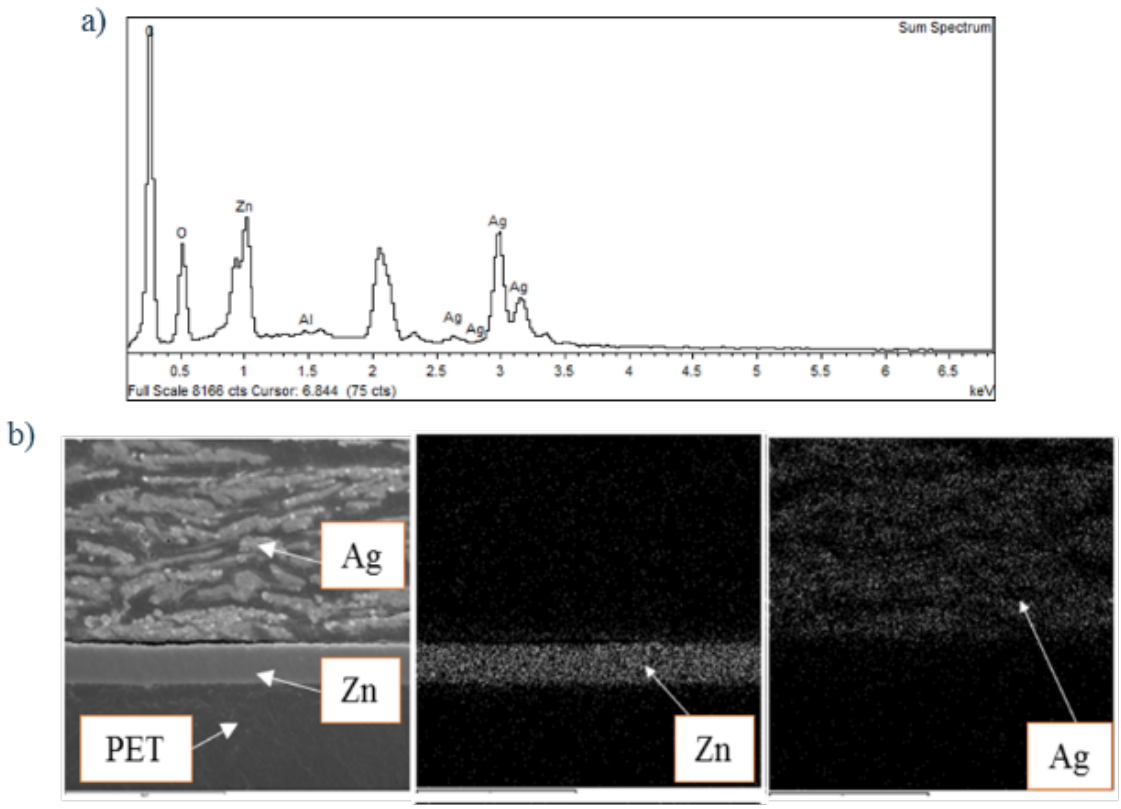

Fig. (14). (**a**) EDS analysis for Ag/AZO/PET (**b**) The EDS distribution area of Zn and Ag.

The sheet resistivity of the silver electrodes and the piezoelectric film were measured using Jandel RM 3000 four-point probe. The screen-printed silver electrodes recorded values of 0.46 – 0.48 Ω.cm. The AZO thin film has resistivities of 0.03 – 0.04 Ω.cm which are within the reported values of 10^{-4} Ω.cm to 10 Ω.cm in literature [124].

3.4. Experimental Measurement of Resonant Frequency and Output Voltage

To validate the theoretical calculations and simulation, an experimental setup for validating the sample was setup as shown in Fig. (**15**). Both the piezoelectric energy harvester and silver electrodes are connected to the Dynamic Signal Analyser. The sample is mounted to a holder and is clamped at one end. The Dynamic Signal Analyser (DSA) functions both as a function generator and as a signal analyser. The power amplifier will amplify the signal generated by DSA before sending it to the electromagnetic shaker. This signal will drive the electromagnetic shaker to vibrate the piezoelectric device at a specific frequency. The generated electricity of the piezoelectric device is then measured using the DSA's signal analyser function.

In this experiment, 12 devices were fabricated on two PET substrates. The devices were cut and measured individually using the setup shown in Fig. (**15**). In this measurement, the input vibrations were swept from 0 to 100 Hz. A sample of the measured output voltage at the DSA is shown in Fig. (**16**). It can be seen that a resonant peak occurs at 49.6 Hz, in which the maximum output voltage of 867.4mV_{rms} was obtained. Measurements of individual devices with different number of IDE pairs and electrode gaps were also performed and their results were summarized in Table **10**.

In this work the devices were fabricated on two separate substrates to evaluate how process variations may affect the performance of the energy harvesters. It can be seen that different substrates will produce different voltage outputs even though both the sputtering conditions (Table **7**) and device dimensions are the same. Substrate 1 consistently shows higher output voltages compared to Substrate 2. This is due to the fact that the both substrates have different surface roughness, resulting in different qualities of AZO thin films. High quality AZO thin films have low surface roughness which lower acoustic loss [121].

It can be seen that devices with larger gap (1.2mm) consistently produce higher output voltage. Similarly, more devices that have more IDE pairs produce larger output voltages compared to devices with less IDE pairs. The measured results were also compared with theoretical calculations based on Equation (4) and COMSOL Simulations as shown in Fig. (**17**). Based on the theoretical calculation, simulation, and measurement, the output voltage can be increased by increasing the number of the IDE pairs and the gap between the electrodes [85, 93]. This was also shown in Table **11**, where the increase in number of IDE pairs results in a large

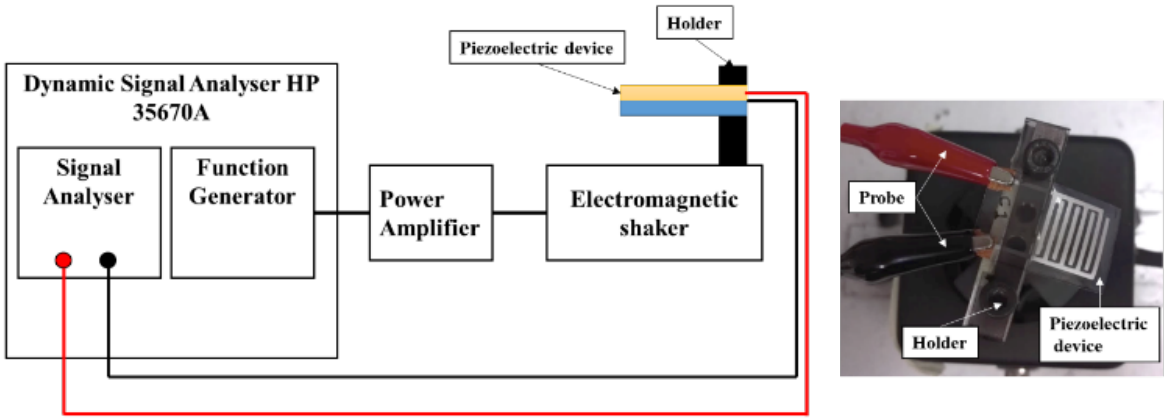

Fig. (15). Left: Experimental setup. Right: Image of flexible energy harvester connected to holder and probes. (*A higher resolution / colour version of this figure is available in the electronic copy of the article*).

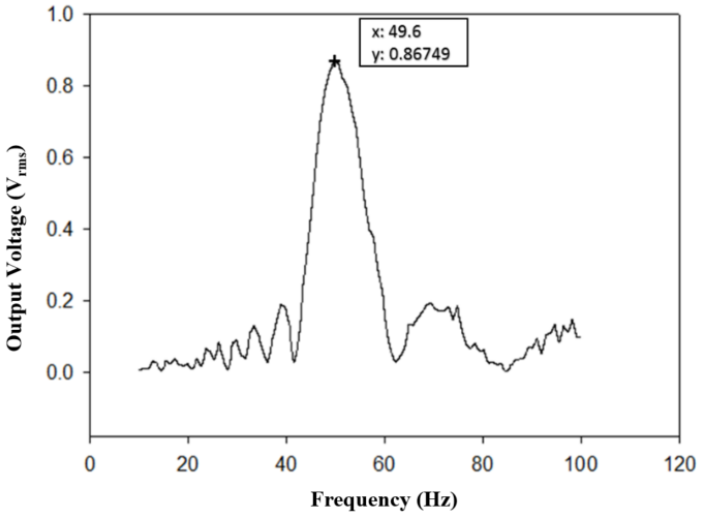

Fig. (16). Frequency versus output voltage of a flexible piezoelectric energy harvester with four IDE pairs.

Table 10. Measured generated output voltages from two different substrates with different number of IDE pairs and different IDE gaps.

Substrate 1		
Number of IDE pairs	**Output Voltage (mV_{rms})**	
	Gap = 1mm	**Gap = 1.2mm**
2	6.736	20.39
3	28.94	29.79
4	637.5	867.4
Substrate 2		
Number of IDE pairs	**Output Voltage (mV_{rms})**	
	Gap = 1mm	Gap = 1.2mm
2	39.87	50.27
3	78.10	97.20
4	126.5	149.8

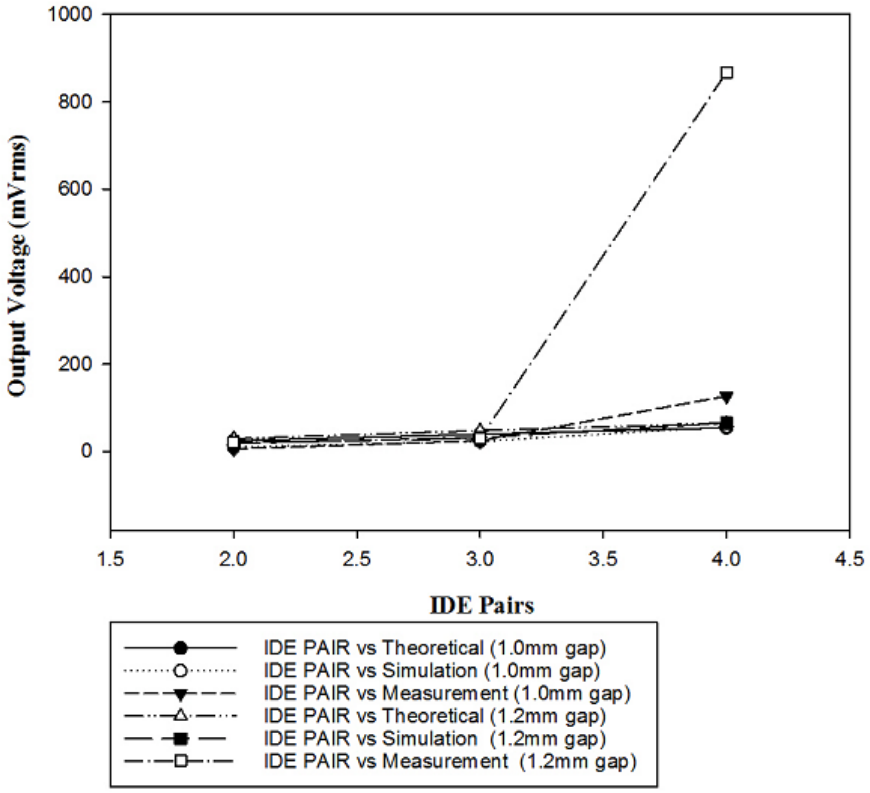

Fig. (17). Comparisons of theoretical, simulation and measurement results for the energy harvesters with 1.0mm and 1.2 mm gaps.

Table 11. Number of IDE pairs versus output voltage.

Number of IDE Pair	Output Voltage (mVrms)		
-	Theoretical	Simulation	Measurement
2	29.686	18.77	20.391
3	47.659	32.39	29.795
4	65.229	65.34	867.45

increase of output voltage. The device with four electrode pairs produces the highest generated voltage of 0.87 V, which is much larger than the simulated values. This is because larger number of electrode pairs allows the structure to capture more bending in the cantilever during vibrations as shown in Fig. (**18**).

Fig **18** (**a**) shows a device with only two IDE pairs which are located near to the tip of the device, covering a small area (136.8 mm^2) of the piezoelectric material during deformations in the z direction. In contrast, Fig **18** (**b**) with four IDE pairs covers a larger area (295.2 mm^2) of piezoelectric material, enabling it to harvest more energy and resulting in higher output voltage. These results are in accordance with [125] which has reported highest strain values near the clamped end of the piezoelectric cantilever beam. In the work done by S. Du et. al [125], they partitioned the electrodes on cantilever beam into 8 different sections and evaluated the generated output at each section. It was shown that the amount of strain decreases in an almost linear fashion with the distance from the clamped end, x. This is in agreement with the findings of our work.

Having increased number of electrodes does not affect the resonant frequency of the cantilever beam as the mass of the electrodes is considered negligible, when compared to the mass of the substrate and the piezoelectric material. Therefore, the calculated resonant frequency of the device with different IDE pairs is the same as shown in Table **12**. The resonant frequency can be controlled by varying the length of the cantilever [126]. Based on theoretical calculation, increasing the length of the cantilever will reduce the resonant frequency.

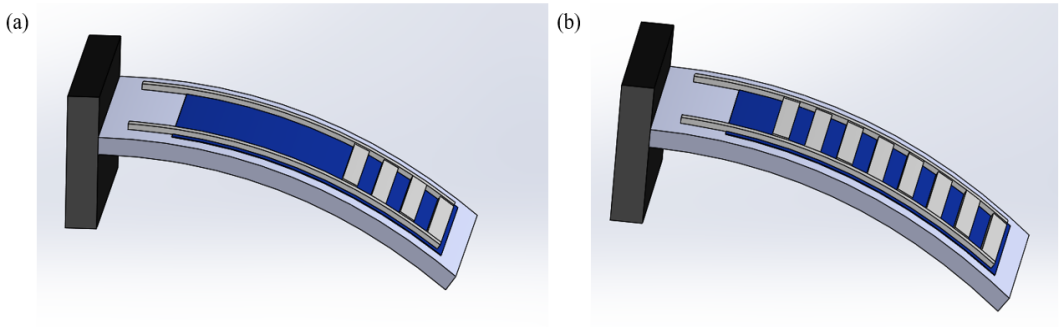

Fig. (18). Illustration of the devices with (**a**) two electrode pairs and (**b**) four electrode pairs during bending at resonance. (*A higher resolution / colour version of this figure is available in the electronic copy of the article*).

Table 12. Theoretical, simulation and measured resonant frequencies.

Number of IDE Pair	Resonant Frequency (Hz)		
	Theoretical	Simulation	Measurement
2	55.54	55.10	50.05
3	55.54	51.70	52.00
4	55.54	48.55	49.60

CONCLUSION

This paper presents the design, simulation, fabrication, and experimental measurement of fabricated piezoelectric energy harvester in d_{33} mode operation. The device has a cantilever structure of PET / AZO / Ag layers. AZO was preferred as a piezoelectric material due to the excellent bonding to the substrate material and its high coefficient of piezoelectric coupling. Simulation analysis was carried out to visualize the resonance frequency as the resonance frequency provides the highest vibration displacement and maximum output power. The output voltage of the piezoelectric device also was simulated using COMSOL. The simulation result shows that the output voltage will be high when the number of IDE pairs and the gap between electrodes high. The proposed designs were developed using RF magnetron sputtering deposition for AZO with optimized parameters and using a screen-printed method for the silver electrode deposition process. Material characterizations were performed using X-ray diffraction (XRD) and field emission scanning electron microscopy (FESEM) with energy dispersive spectroscopy (EDS) to evaluate the piezoelectric qualities and surface morphology with element analysis, respectively. The c-axis orientation of AZO at 002 peak was clearly shown at 2 θ values of 34.45° which is very close with pure ZnO orientation. The fabricated device was tested to measure the output voltage produced. The results indicate approximately 0.867 V_{rms} output voltage is produced at 49.6 Hz resonance frequency

CONSENT FOR PUBLICATION

Not applicable.

AVAILABILITY OF DATA AND MATERIALS

Not applicable.

FUNDING

This work is a collaborative research between International Islamic University Malaysia (IIUM) and Jabil Circuits Sdn. Bhd. The research is co-funded by Jabil Circuits and IIUM under P-RIGS18-038-0038.

CONFLICT OF INTEREST

The authors declare no conflict of interest, financial or otherwise.

ACKNOWLEDGEMENTS

Declared None.

REFERENCES

[1] Iranmanesh S, Raikos G, Imtiaz SA, Rodriguez-Villegas E. A Seizure-Based Power Reduction SoC for Wearable EEG in Epilepsy. IEEE Access 2019; 7: 151682-91. http://dx.doi.org/10.1109/ACCESS.2019.2948231

[2] Kalantarian H, Sideris C, Mortazavi B, Alshurafa N, Sarrafzadeh M. Dynamic Computation Offloading for Low-Power Wearable Health Monitoring Systems. IEEE Trans Biomed Eng 2017; 64(3): 621-8. http://dx.doi.org/10.1109/TBME.2016.2570210 PMID: 28113209

[3] Spanò E, Di Pascoli S, Iannaccone G. Low-Power Wearable ECG Monitoring System for Multiple-Patient Remote Monitoring. IEEE Sens J 2016; 16(13): 5452-62. http://dx.doi.org/10.1109/JSEN.2016.2564995

[4] Ashyap AYI, *et al.* Compact and Low-Profile Textile EBG-Based Antenna for Wearable Medical Applications. IEEE Antennas Wirel Propag Lett 2017; 16(c): 2550-3.

http://dx.doi.org/10.1109/LAWP.2017.2732355

[5] Kim J, Gutruf P, Chiarelli AM, *et al.* Miniaturized Battery-Free Wireless Systems for Wearable Pulse Oximetry. Adv Funct Mater 2017; 27(1): 1-8. http://dx.doi.org/10.1002/adfm.201604373 PMID: 28798658

[6] Kim J, *et al.* Miniaturized Flexible Electronic Systems with Wireless Power and Near-Field Communication Capabilities. Adv Funct Mater 2015; 25(30): 4761-7. http://dx.doi.org/10.1002/adfm.201501590

[7] Mallires KR, Wang D, Tipparaju VV, Tao N. Developing a Low-Cost Wearable Personal Exposure Monitor for Studying Respiratory Diseases Using Metal-Oxide Sensors. IEEE Sens J 2019; 19(18): 8252-61. http://dx.doi.org/10.1109/JSEN.2019.2917435

[8] Xuan X, Yoon HS, Park JY. A wearable electrochemical glucose sensor based on simple and low-cost fabrication supported micropatterned reduced graphene oxide nanocomposite electrode on flexible substrate. Biosens Bioelectron 2018; 109: 75-82. http://dx.doi.org/10.1016/j.bios.2018.02.054 PMID: 29529511

[9] Saleh M, Jeannes RLB. Elderly Fall Detection Using Wearable Sensors: A Low Cost Highly Accurate Algorithm. IEEE Sens J 2019; 19(8): 3156-64. http://dx.doi.org/10.1109/JSEN.2019.2891128

[10] Dierk C, Nicholas MJP, Paulos E. AlterWear: Battery-free wearable displays for opportunistic interactions Conf Hum Factors Comput Syst - Proc 2018; 1-11. http://dx.doi.org/10.1145/3173574.3173794

[11] Talla V, Pellerano S, Xu H, Ravi A, Palaskas Y. Wi-Fi RF energy harvesting for battery-free wearable radio platforms 2015 IEEE Int Conf RFID, RFID 2015. 47-54. http://dx.doi.org/10.1109/RFID.2015.7113072

[12] Hester J, Storer K, Sorber J. Timely execution on intermittently powered batteryless sensors SenSys 2017 - Proc 15th ACM Conf Embed Networked Sens Syst. http://dx.doi.org/10.1145/3131672.3131673

[13] Çakıroğlu B, Özacar M. A self-powered photoelectrochemical glucose biosensor based on supercapacitor Co_3O_4-CNT hybrid on TiO_2. Biosens Bioelectron 2018; 119: 34-41. http://dx.doi.org/10.1016/j.bios.2018.07.049 PMID: 30098464

[14] Huang M, Zhou C, Tian J, Yang K, Yang H, Lu J. Self-powered aptasensing for prostate specific antigen based on a membraneless photoelectrochemical fuel cell. Biosens Bioelectron 2020; 165(May) http://dx.doi.org/10.1016/j.bios.2020.112357 PMID: 32729490

[15] Cho E, Mohammadifar M, Choi S. A SELF-POWERED SENSOR PATCH FOR GLUCOSE MONITORING IN SWEAT 2017 IEEE 30th International Conference on Micro Electro Mechanical Systems (MEMS). 366-9. http://dx.doi.org/10.1109/MEMSYS.2017.7863417

[16] Jeerapan I, Sempionatto JR, Wang J. On-Body Bioelectronics : Wearable Biofuel Cells for Bioenergy Harvesting and Self-Powered Biosensing. Adv Funct Mater 2019; 1906243: 1-18. http://dx.doi.org/10.1002/adfm.201906243

[17] Shitanda I, Soc JE, Shitanda I, Fujimura Y, Nohara S, Hoshi Y. Paper-Based Disk-Type Self-Powered Glucose Biosensor Based on Screen-Printed Biofuel Cell Array Paper-Based Disk-Type Self-Powered Glucose Biosensor Based on Screen-Printed Biofuel Cell Array. J Electrochem Soc 2019; 166(12): B1063-8. http://dx.doi.org/10.1149/2.1501912jes

[18] Babar M, Rahman A, Arif F, Jeon G. Energy-harvesting based on internet of things and big data analytics for smart health monitoring. Sustain Comput Informatics Syst 2018; 20: 155-64. http://dx.doi.org/10.1016/j.suscom.2017.10.009

[19] Yan C, *et al.* A linear-to-rotary hybrid nanogenerator for high-performance wearable biomechanical energy harvesting. Nano Energy 2020; 67 http://dx.doi.org/10.1016/j.nanoen.2019.104235

[20] Ibarra E, Antonopoulos A, Kartsakli E, Rodrigues JJPC, Verikoukis C. QoS-Aware Energy Management in Body Sensor Nodes Powered by Human Energy Harvesting. IEEE Sens J 2016; 16(2): 542-9. http://dx.doi.org/10.1109/JSEN.2015.2483064

[21] Iqbal M, Khan FU. Hybrid vibration and wind energy harvesting using combined piezoelectric and electromagnetic conversion for bridge health monitoring applications. Energy Convers Manage 2018; 172(July): 611-8. http://dx.doi.org/10.1016/j.enconman.2018.07.044

[22] Le MQ, *et al.* Review on energy harvesting for structural health monitoring in aeronautical applications. Prog Aerosp Sci 2015; 79: 147-57. http://dx.doi.org/10.1016/j.paerosci.2015.10.001

[23] Maruccio C, Quaranta G, De Lorenzis L, Monti G. Energy harvesting from electrospun piezoelectric nanofibers for structural health monitoring of a cable-stayed bridge. Smart Mater Struct 2016; 25(8): 1-13. http://dx.doi.org/10.1088/0964-1726/25/8/085040

[24] Sharma H, Haque A, Jaffery ZA. Maximization of wireless sensor network lifetime using solar energy harvesting for smart agriculture monitoring. Ad Hoc Netw 2019; 94 http://dx.doi.org/10.1016/j.adhoc.2019.101966

[25] Sharma H, Haque A, Jaffery ZA. Smart Agriculture Monitoring using Energy Harvesting Internet of Things (EH-IoT). World Sci News 2019; 121(February): 22-6.

[26] Zergoune Z, Kacem N, Bouhaddi N. On the energy localization in weakly coupled oscillators for electromagnetic vibration energy harvesting. Smart Mater Struct 2019; 28(7) http://dx.doi.org/10.1088/1361-665X/ab05f8

[27] Ozger M, Cetinkaya O, Akan OB. Energy Harvesting Cognitive Radio Networking for IoT-enabled Smart Grid. Mob Netw Appl 2018; 23(4): 956-66. http://dx.doi.org/10.1007/s11036-017-0961-3

[28] Zhao Z, *et al.* Analysis and application of the piezoelectric energy harvester on light electric logistics vehicle suspension systems. Energy Sci Eng 2019; 7(6): 2741-55. http://dx.doi.org/10.1002/ese3.456

[29] Tentzeris MM, Georgiadis A, Roselli L. Energy Harvesting and Scavenging [Scanning the Issue]. Proc IEEE 2014; 102(11): 1644-8. http://dx.doi.org/10.1109/JPROC.2014.2361599

[30] Pang Y, Ding H, Liu J, Fang Y, Chen S. A UHF RFID-Based System for Children Tracking. IEEE Internet Things J 2018; 5(6): 5055-64. http://dx.doi.org/10.1109/JIOT.2018.2841809

[31] Manyala RO. Introductory Chapter: Trends in Research on Energy Harvesting Technology. Energy Harvest 2018; pp. 1-4.

[32] Tan YK. *SUSTAINABLE ENERGY HARVESTING TECHNOLOGIES – PAST, Edited by Yen Kheng Tan*. 2011.

[33] Zhou Y, Zhang S, Ding Y, Zhang L, Zhang C, Zhang X. Efficient Solar Energy Harvesting and Storage through a Robust Photocatalyst Driving Reversible Redox Reactions. 2018; Vol. 1802294: pp. 1-7.

[34] Chai Z, Zhang N, Sun P, *et al.* Tailorable and Wearable Textile Devices for Solar Energy Harvesting and Simultaneous Storage. ACS Nano 2016; 10(10): 9201-7. http://dx.doi.org/10.1021/acsnano.6b05293 PMID: 27701868

[35] Sharma H, Haque A, Jaffery ZA. Solar energy harvesting wireless sensor network nodes: A survey. J Renew Sustain Energy 2018; 10(2) http://dx.doi.org/10.1063/1.5006619

[36] Liu J, Jia Y, Jiang Q, *et al.* Highly Conductive Hydrogel Polymer Fibers toward Promising Wearable Thermoelectric Energy Harvesting. ACS Appl Mater Interfaces 2018; 10(50): 44033-40. http://dx.doi.org/10.1021/acsami.8b15332 PMID: 30523679

[37] Nozariasbmarz A, *et al.* Review of wearable thermoelectric energy harvesting: From body temperature to electronic systems. Appl Energy 2020; 258(April) http://dx.doi.org/10.1016/j.apenergy.2019.114069

[38] Yang Y, Guo W, Pradel KC, *et al.* Pyroelectric nanogenerators for harvesting thermoelectric energy. Nano Lett 2012; 12(6): 2833-8. http://dx.doi.org/10.1021/nl3003039 PMID: 22545631

[39] Chen Z, Xia Y, He J, Xiong Y, Wang G. Elastic-electro-mechanical modeling and analysis of piezoelectric metamaterial plate with a self-powered synchronized charge extraction circuit for vibration energy harvesting. Mech Syst Signal Process 2020; 143 http://dx.doi.org/10.1016/j.ymssp.2020.106824

[40] Abdelkareem MAA, *et al.* Vibration energy harvesting in automotive suspension system: A detailed review. Appl Energy 2018; 229(August): 672-99.

http://dx.doi.org/10.1016/j.apenergy.2018.08.030

[41] Kim HS, Kim JH, Kim J. A review of piezoelectric energy harvesting based on vibration. Int J Precis Eng Manuf 2011; 12(6): 1129-41.
http://dx.doi.org/10.1007/s12541-011-0151-3

[42] Divakaran S K, Das Krishna D. RF energy harvesting systems: An overview and design issues. Int J RF Microw Comput Eng 2019; 29(1): 1-15.

[43] Assogba O, Mbodji AK, Karim Diallo A. Efficiency in RF energy harvesting systems: A comprehensive review IBASE-BF 2020 - 1st IEEE Int Conf Nat Eng Sci Sahel Sustain Dev Impact Big Data Appl Soc Environ. 1-10.
http://dx.doi.org/10.1109/IBASE-BF48578.2020.9069597

[44] Visser HJ, Vullers RJM. RF energy harvesting and transport for wireless sensor network applications: Principles and requirements. Proc IEEE 2013; 101(6): 1410-23.
http://dx.doi.org/10.1109/JPROC.2013.2250891

[45] La Rosa R, Livreri P, Trigona C, Di Donato L, Sorbello G. Strategies and techniques for powering wireless sensor nodes through energy harvesting and wireless power transfer. Sensors 2019; 19(12)
http://dx.doi.org/10.3390/s19122660

[46] Zareei S, Deng JD. "Energy harvesting modelling for self-powered fitness gadgets: a feasibility study," *Int. J. Parallel*. Emergent Distrib Syst 2019; 34(4): 412-29.
http://dx.doi.org/10.1080/17445760.2017.1410817

[47] Basaloom AAS, Hadi Habaebi M, Khan S, Shaikh FA. Increasing RPL-based LLN Lifespan using Harvested Solar Energy 2019 IEEE International Conference on Smart Instrumentation, Measurement and Application (ICSIMA). 1-6.

[48] Jiang X, Polastre J, Culler D. Perpetual environmentally powered sensor networks 2005 4th Int Symp Inf Process Sens Networks, IPSN 2005. 463-8.

[49] Roundy S, Otis BP, Chee Y-H, Rabaey JM, Wright P. A 1.9 GHz RF transmit beacon using environmentally scavenged energy. Optimization 2003; 4(2): 4.

[50] Tian R, *et al.* A solution-processed TiS2/organic hybrid superlattice film towards flexible thermoelectric devices. J Mater Chem A Mater Energy Sustain 2017; 5(2): 564-70.
http://dx.doi.org/10.1039/C6TA08838D

[51] Choi K, Ahn D, Boo JH. Influence of temperature gradient induced by concentrated solar thermal energy on the power generation performance of a thermoelectric module. J Korea Acad Coop Soc 2017; 18(10): 777-84.

[52] Böttner H, *et al.* New thermoelectric components using microsystems technologies. J Microelectromech Syst 2004; 13(3): 414-20.
http://dx.doi.org/10.1109/JMEMS.2004.828740

[53] Fan K, Cai M, Liu H, Zhang Y. Capturing energy from ultra-low frequency vibrations and human motion through a monostable electromagnetic energy harvester. Energy 2019; 169: 356-68.
http://dx.doi.org/10.1016/j.energy.2018.12.053

[54] Nia EM, Zawawi NAWA, Singh BSM. A review of walking energy harvesting using piezoelectric materials IOP Conf Ser Mater Sci Eng. vol. 291

[55] Khalatkar AM, Gupta VK. Piezoelectric energy harvester for low engine vibrations. J Renew Sustain Energy 2017; 9(2)
http://dx.doi.org/10.1063/1.4979501

[56] Roundy S, Wright PK, Rabaey J. A study of low level vibrations as a power source for wireless sensor nodes. Comput Commun 2003; 26(11): 1131-44.
http://dx.doi.org/10.1016/S0140-3664(02)00248-7

[57] Carneiro P, *et al.* Electromagnetic energy harvesting using magnetic levitation architectures: A review. Appl Energy 2020; 260: 114191.
http://dx.doi.org/10.1016/j.apenergy.2019.114191

[58] Li Z, Zuo L, Luhrs G, Lin L, Qin YX. Electromagnetic energy-harvesting shock absorbers: Design, modeling, and road tests. IEEE Trans Vehicular Technol 2013; 62(3): 1065-74.
http://dx.doi.org/10.1109/TVT.2012.2229308

[59] Guo X, Zhang Y, Fan K, Lee C, Wang F. A comprehensive study of non-linear air damping and 'pull-in' effects on the electrostatic energy harvesters. Energy Convers Manage 2020; 203(June)
http://dx.doi.org/10.1016/j.enconman.2019.112264

[60] Boisseau S, Despesse G, Ahmed B. Electrostatic Conversion for Vibration Energy Harvesting. Small-Scale Energy Harvest 2012.
http://dx.doi.org/10.5772/51360

[61] Priya S, *et al.* A Review on Piezoelectric Energy Harvesting: Materials, Methods, and Circuits. Energy Harvest Syst 2017; 4(1): 3-39.
http://dx.doi.org/10.1515/ehs-2016-0028

[62] Ralib AAM, Nordin AN, Othman R, Salleh H. Design, simulation and fabrication of piezoelectric micro generators for aero acoustic applications. Microsyst Technol 2011; 17(4): 563-73.
http://dx.doi.org/10.1007/s00542-011-1228-8

[63] Meninger S, Mur-miranda JO, Amirtharajah R, Chandrakasan AP, Lang JH. Vibration-to-Electric Energy Conversion 2001; 9(1): 64-76.

[64] Oza V, *et al.* Development of an electromagnetic micro-generator. J Qual Technol Manag 2007; 20(3–4): 87-97.

[65] Beeby SP, Tudor MJ, White NM. Energy harvesting vibration sources for microsystems applications. Meas Sci Technol 2006; 17(12): R175-95.
http://dx.doi.org/10.1088/0957-0233/17/12/R01

[66] Choi WJ, Jeon Y, Jeong JH, Sood R, Kim SG. Energy harvesting MEMS device based on thin film piezoelectric cantilevers. J Electroceram 2006; 17(2–4): 543-8.
http://dx.doi.org/10.1007/s10832-006-6287-3

[67] Paradiso JA, Starner T. Energy scavenging for mobile and wireless electronics. IEEE Pervasive Comput 2005; 4(1): 18-27.
http://dx.doi.org/10.1109/MPRV.2005.9

[68] Covaci C, Gontean A. Piezoelectric energy harvesting solutions: A review. Sensors (Basel) 2020; 20(12): 1-37.
http://dx.doi.org/10.3390/s20123512 PMID: 32575888

[69] Zhou H, Zhang Y, Qiu Y, *et al.* Stretchable piezoelectric energy harvesters and self-powered sensors for wearable and implantable devices. Biosens Bioelectron 2020; 168(May)
http://dx.doi.org/10.1016/j.bios.2020.112569 PMID: 32905930

[70] Carbonaro N, Lorussi F, Tognetti A. Assessment of a smart sensing shoe for gait phase detection in level walking. Electron 2016; 5(4): 1-15.
http://dx.doi.org/10.3390/electronics5040078

[71] Eskofier BM, *et al.* An overview of smart shoes in the internet of health things: Gait and mobility assessment in health promotion and disease monitoring. Appl Sci (Basel) 2017; 7(10)
http://dx.doi.org/10.3390/app7100986

[72] Badawi H, Laamarti F, Arafsha F, El Saddik A. Standardizing a Shoe Insole Based on ISO/IEEE 11073 Personal Health Device (X73-PHD) StandardsAdvances in Intelligent Systems and Computing. Springer International Publishing. 2019; pp. 918764-78.
http://dx.doi.org/10.1007/978-3-030-11890-7_72

[73] Tabrizi MM, Sharifnezhad A, Agheli M. Development of a totally embedded smart insole Proc ASME Des Eng Tech Conf. 1-5.
http://dx.doi.org/10.1115/DETC2018-86399

[74] Lamaarti F, Arafsha F, Hafidh B, El Saddik A. Automated Athlete Haptic Training System for Soccer Sprinting 2nd Int Conf Multimed Inf Process Retrieval, MIPR 2019. 303-9.
http://dx.doi.org/10.1109/MIPR.2019.00061

[75] Mehendale N, Gokalgandhi D, Shah N, Kamdar L. A Review of Smart Technologies Embedded in Shoes. SSRN Electron. J. 2020; pp. 1-9.

[76] Geisler M, *et al.* Human-motion energy harvester for autonomous body area sensors Smart Mater Struct 2017; 26(3): 0-31.
http://dx.doi.org/10.1088/1361-665X/aa548a

[77] Kohiki S, Nishitani M, Wada T. Enhanced electrical conductivity of zinc oxide thin films by ion implantation of gallium, aluminum, and boron atoms. J Appl Phys 1994; 75(4): 2069-72.
http://dx.doi.org/10.1063/1.356310

[78] Halim MA, Cho H, Park JY. Design and experiment of a human-limb driven, frequency up-converted electromagnetic energy harvester. Energy Convers Manage 2015; 106: 393-404.
http://dx.doi.org/10.1016/j.enconman.2015.09.065

[79] Cho KH, Shin DJ, Lee CS, Koh JH. Impedance Matching Techniques of Multi-layered PZT Ceramics for Piezoelectric Energy Harvesters. Electron Mater Lett 2019; 15(4): 437-43.
http://dx.doi.org/10.1007/s13391-019-00135-w

[80] Almusallam A, Torah RN, Zhu D, Tudor MJ, Beeby SP. Screen-printed piezoelectric shoe-insole energy harvester using an im-

proved flexible PZT-polymer composites. J Phys Conf Ser 2013; 476(1): 12108.
http://dx.doi.org/10.1088/1742-6596/476/1/012108

[81] Tao K, *et al.* Piezoelectric ZnO thin films for 2DOF MEMS vibrational energy harvesting. Surf Coat Tech 2019; 359: 289-95.
http://dx.doi.org/10.1016/j.surfcoat.2018.11.102

[82] Han D, *et al.* Fabrication and characteristics of ZnO thin films deposited by RF sputtering on plastic substrates for flexible display. Sci China Inf Sci 2012; 55(6): 1441-5.
http://dx.doi.org/10.1007/s11432-011-4348-y

[83] Wasa K, Kanno I, Kotera H. Fundamentals of thin film piezoelectric materials and processing design for a better energy harvesting MEMS. Power MEMS 2009; 61: 61-6.

[84] Gablech I, Klempa J, Pekárek J, *et al.* Simple and efficient AlN-Based piezoelectric energy harvesters. Micromachines (Basel) 2020; 11(2): 1-10.
http://dx.doi.org/10.3390/mi11020143 PMID: 32012859

[85] Shen Z, Liu S, Miao J, Woh LS, Wang Z. Spiral electrode d33 mode piezoelectric diaphragm combined with proof mass as energy harvester. J Micromech Microeng 2015; 25(3)
http://dx.doi.org/10.1088/0960-1317/25/3/035004

[86] Chin HS, Chao LS, Wu CC. Crystal, optical, and electrical characteristics of transparent conducting gallium-doped zinc oxide films deposited on flexible polyethylene naphthalate substrates using radio frequency magnetron sputtering. Mater Res Bull 2016; 79: 90-6.
http://dx.doi.org/10.1016/j.materresbull.2016.03.017

[87] Nomoto J, Makino H, Nakajima T, Tsuchiya T, Yamamoto T. Improvement of the Properties of Direct-Current Magnetron-Sputtered Al-Doped ZnO Polycrystalline Films Containing Retained Ar Atoms Using 10-nm-Thick Buffer Layers. ACS Omega 2019; 4(11): 14526-36.
http://dx.doi.org/10.1021/acsomega.9b01761 PMID: 31528807

[88] Zhu C, Zhou T, Shi F, Song W, Li J, Wu W. Room-temperature RF magnetron sputtering deposition of hydrogenated Ga-doped ZnO thin films on PET substrates for PDLC devices. Appl. Phys. A Mater. Sci. Process.2018; 124(12):
http://dx.doi.org/10.1007/s00339-018-2276-z

[89] Pan C T. Design and Fabrication of Flexible Piezoelectric Generators Based on ZnO Thin Films 2014.
http://dx.doi.org/10.1002/9781118487808.ch2

[90] El Hamali SO, Cranton WM, Kalfagiannis N, Hou X, Ranson R, Koutsogeorgis DC. Enhanced electrical and optical properties of room temperature deposited Aluminium doped Zinc Oxide (AZO) thin films by excimer laser annealing. Opt Lasers Eng 2016; 80: 45-51.
http://dx.doi.org/10.1016/j.optlaseng.2015.12.010

[91] Md Ralib AA, Nordin AN, Salleh H, Othman R. Fabrication of aluminium doped zinc oxide piezoelectric thin film on a silicon substrate for piezoelectric MEMS energy harvesters. Microsyst Technol 2012; 18(11): 1761-9.
http://dx.doi.org/10.1007/s00542-012-1550-9

[92] Jeong D, Kang C, Priya S. Ultra-Low Resonant Piezoelectric MEMS Energy Harvester With High Power Density. J Microelectromechanical Syst 2017; (99): 1-9.

[93] Zhao J, You Z. A shoe-embedded piezoelectric energy harvester for wearable sensors. Sensors (Basel) 2014; 14(7): 12497-510.
http://dx.doi.org/10.3390/s140712497 PMID: 25019634

[94] Jung WS, *et al.* Powerful curved piezoelectric generator for wearable applications. Nano Energy 2015; 13: 174-81.
http://dx.doi.org/10.1016/j.nanoen.2015.01.051

[95] Nishi T, Ito T, Hida H, Kanno I. Shoe-mounted vibration energy harvester of PZT piezoelectric thin films on metal foils. J Phys Conf Ser 2016; 773
http://dx.doi.org/10.1088/1742-6596/773/1/012062

[96] Pan CT, Liu ZH, Chen YC, Liu CF. Design and fabrication of flexible piezo-microgenerator by depositing ZnO thin films on PET substrates. Sens Actuators A Phys 2010; 159(1): 96-104.
http://dx.doi.org/10.1016/j.sna.2010.02.023

[97] Yang Y, Wang S, Stein P, Xu BX, Yang T. Vibration-based energy harvesting with a clamped piezoelectric circular diaphragm: Analysis and identification of optimal structural parameters. Smart Mater Struct 2017; 26(4)
http://dx.doi.org/10.1088/1361-665X/aa5fda

[98] Zhao Q, Liu Y, Wang L, Yang H, Cao D. Design method for piezoelectric cantilever beam structure under low frequency condition. Int J Pavement Res Technol 2018; 11(2): 153-9.
http://dx.doi.org/10.1016/j.ijprt.2017.08.001

[99] Usharani R, Uma G, Umapathy M. "Design of high output broadband piezoelectric energy harvester with double tapered cavity beam," *Int. J. Precis. Eng. Manuf.* -. Green Technol 2016; 3(4): 343-51.

[100] Tang G, Yang B, Liu JQ, Xu B, Zhu HY, Yang CS. Development of high performance piezoelectric d33mode MEMS vibration energy harvester based on PMN-PT single crystal thick film. Sens Actuators A Phys 2014; 205: 150-5.
http://dx.doi.org/10.1016/j.sna.2013.11.007

[101] Priya S, Inman DJ. Energy harvesting technologies. Springer 2009; Vol. 21.
http://dx.doi.org/10.1007/978-0-387-76464-1

[102] Shivashankar P, Gopalakrishnan S. Design, modeling and testing of d33-mode surface-bondable multilayer piezoelectric actuator. Smart Mater Struct 2020; 29(4)
http://dx.doi.org/10.1088/1361-665X/ab6698

[103] Zhou H, Han RH, Xu MH, Guo H. Study of a piezoelectric accelerometer based on d33 mode Proc 2016 Symp Piezoelectricity, Acoust Waves Device Appl SPAWDA 2016. 61-5.

[104] Park JC, Member S, Park JY, Lee Y. Modeling and Characterization of Piezoelectric d 33 -Mode MEMS Energy Harvester. 2010; 19: pp. (5)1215-22.
http://dx.doi.org/10.1109/JMEMS.2010.2067431

[105] Hosseini R, Hamedi M. An investigation into resonant frequency of trapezoidal V-shaped cantilever piezoelectric energy harvester. Microsyst Technol 2016; 22(5): 1127-34.
http://dx.doi.org/10.1007/s00542-015-2583-7

[106] Hegde N, Bries M, Sazonov E. A Comparative Review of Footwear-Based Wearable Systems. Electronics (Basel) 2016; 5(48): 1-28.
http://dx.doi.org/10.3390/electronics5030048

[107] Guan M, Liao WH. Design and analysis of a piezoelectric energy harvester for rotational motion system. Energy Convers Manage 2016; 111: 239-44.
http://dx.doi.org/10.1016/j.enconman.2015.12.061

[108] Wang L, *et al.* High accuracy comsol simulation method of bimorph cantilever for piezoelectric vibration energy harvesting. AIP Adv 2019; 9(9)
http://dx.doi.org/10.1063/1.5119328

[109] Alsaad AM, Ahmad AA, Al-Bataineh QM, Daoud NS, Khazaleh MH. Design and Analysis of MEMS Based Aluminum Nitride (AlN), Lithium Niobate (LiNbO3) and Zinc Oxide (ZnO) Cantilever with Different Substrate Materials for Piezoelectric Vibration Energy Harvesters Using COMSOL Multiphysics Software. Open J Appl Sci 2019; 09(04): 181-97.
http://dx.doi.org/10.4236/ojapps.2019.94016

[110] Yeo HG, Xue T, Roundy S, Ma X, Rahn C, Trolier-McKinstry S. Strongly (001) Oriented Bimorph PZT Film on Metal Foils Grown by rf-Sputtering for Wrist-Worn Piezoelectric Energy Harvesters. Adv Funct Mater 2018; 28(36): 1-9.
http://dx.doi.org/10.1002/adfm.201801327

[111] Han CS, Lee TH, Kim GM, Lee DY, Cho YS. Piezoelectric energy harvesting characteristics of GaN nanowires prepared by a magnetic field-assisted CVD process. J Korean Ceram Soc 2016; 53(2): 167-70.
http://dx.doi.org/10.4191/kcers.2016.53.2.167

[112] Praveen JP, Karthik T, James AR, Chandrakala E, Asthana S, Das D. Effect of poling process on piezoelectric properties of sol-gel derived BZT-BCT ceramics. J Eur Ceram Soc 2015; 35(6): 1785-98.
http://dx.doi.org/10.1016/j.jeurceramsoc.2014.12.010

[113] Ralib AAM, Mortada O, Orlianges JC, Crunteanu A, Chatras M, Nordin AN. Enhanced piezoelectric properties of aluminium doped zinc oxide thin film for surface acoustic wave resonators on a CMOS platform. J Mater Sci Mater Electron 2017; 28(12): 9132-8.
http://dx.doi.org/10.1007/s10854-017-6647-6

[114] Zhang Y, Jiang X, Zhang J, Zhang H, Li Y. Simultaneous voltammetric determination of acetaminophen and isoniazid using MXene modified screen-printed electrode. Biosens Bioelectron 2019; 130(January): 315-21.

http://dx.doi.org/10.1016/j.bios.2019.01.043 PMID: 30784985

[115] Hyun WJ, Lim S, Ahn BY, Lewis JA, Frisbie CD, Francis LF. Screen Printing of Highly Loaded Silver Inks on Plastic Substrates Using Silicon Stencils. ACS Appl Mater Interfaces 2015; 7(23): 12619-24.
http://dx.doi.org/10.1021/acsami.5b02487 PMID: 26035226

[116] Chen Y, *et al.* Polarization-Enhanced direct Z-scheme ZnO-WO3-x nanorod arrays for efficient piezoelectric-photoelectrochemical Water splitting. Appl Catal B 2019; 259(August)
http://dx.doi.org/10.1016/j.apcatb.2019.118079

[117] Jain P, *et al.* Switchable electric polarization and ferroelectric domains in a metal-organic-framework npj Quantum Mater 2016; 11-6.
http://dx.doi.org/10.1038/npjquantmats.2016.12

[118] Epp J. X-Ray Diffraction (XRD) Techniques for Materials Characterization. Elsevier Ltd 2016.
http://dx.doi.org/10.1016/B978-0-08-100040-3.00004-3

[119] Park JH. Deposition-Temperature Effects on AZO Thin Films Prepared by RF Magnetron Sputtering and Their Physical Properties 2006; 49(December): 584-8.

[120] Gâlc AC, Secu M, Vlad A, Pedarnig JD. Optical properties of zinc oxide thin fi lms doped with aluminum and lithium. 2010; Vol. 518: pp. 4603-6.

[121] Kumar A, Saini SK, Sharma G, Johar AK. Development and characterization of ZnO thin film for piezoelectric applications Mater. Today Proc.2020; (xxxx): 1-3.
http://dx.doi.org/10.1016/j.matpr.2020.01.351

[122] Liu SJ, Wan B, Wang P, Song SH. Influence of A-site non-stoichiometry on structure and electrical properties of K0.5Na0.5NbO3-based lead-free piezoelectric ceramics. Scr Mater 2010; 63(1): 124-7.
http://dx.doi.org/10.1016/j.scriptamat.2010.03.033

[123] Wang P, Du H, Shen S, Zhang M, Liu B. Applied Surface Science Deposition, characterization and optimization of zinc oxide thin film for piezoelectric cantilevers. Appl Surf Sci 2012; 258(24): 9510-7.
http://dx.doi.org/10.1016/j.apsusc.2012.04.158

[124] David T, Goldsmith S, Boxman RL. Dependence of zinc oxide thin film properties on filtered vacuum arc deposition parameters. J Phys D Appl Phys 2005; 38(14): 2407-16.
http://dx.doi.org/10.1088/0022-3727/38/14/017

[125] Du S, *et al.* A new electrode design method in piezoelectric vibration energy harvesters to maximize output power. Sens Actuators A Phys 2017; 263: 693-701.
http://dx.doi.org/10.1016/j.sna.2017.06.026

[126] Jamain UM, Ibrahim NH, Rahim RA. Performance analysis of zinc oxide piezoelectric MEMS energy harvester IEEE Int Conf Semicond Electron Proceedings, ICSE. 263-6.
http://dx.doi.org/10.1109/SMELEC.2014.6920847